TECHNICAL NOTE

D-83

MIXING OF WAKES IN A TURBULENT SHEAR FLOW

By Salamon Eskinazi
Syracuse University

NATIONAL AERONAUTICS AND SPACE ADMINISTRATION
WASHINGTON September 1959

NATIONAL AERONAUTICS AND SPACE ADMINISTRATION

TECHNICAL NOTE D-83

MIXING OF WAKES IN A TURBULENT SHEAR FLOW

By Salamon Eskinazi

SUMMARY

Measurements were taken in the wake of a two-dimensional cylinder placed in a fully developed turbulent viscous layer inside a two-dimensional channel. The experimental survey consisted mainly of temporal mean velocity, static-pressure distributions, turbulence velocity, and scale measurements. The survey pertains to cylinder positions across the layer ranging from 0.072 to 0.5 of the channel width for positions downstream of the wire from 5 to 1,000 wire diameters. In the temporal-mean-velocity distribution, the mixing process showed transverse similarities to the free-stream mixing of turbulent and laminar wakes. The longitudinal rate of mixing of the wake at the center of the channel is larger than that in a free stream with low turbulence levels, and when the wake is near the wall the rate of mixing is even greater. Some discussions are included concerning the process of decay, when the wire is very near the wall and the wake spreads to the wall. The Reynolds number of the flow in the channel based on the half-width of the channel and the space mean velocity is 86,000, and that of the cylinder based on its diameter and the space mean velocity is 2,240.

INTRODUCTION

The decay of unrestricted shear flows originating from velocity discontinuities produced by jets, wakes, and cavities has been of considerable interest in the past years. Most of the work performed on this subject, whether analytical, semiempirical, or experimental, deals with the study of shear flows generated in free streams with low turbulence levels. The analytical and semiempirical approaches to the solution of laminar or turbulent jets and wakes are all based on the view that there is a region downstream of the disturbance or nozzle mouth where the mean flow assumes a lateral universal distribution. Experimental investigations rightfully do justify this assumption. Furthermore, the universal character of the mean flow in the lateral direction has been experimentally shown to be unique whether it pertains to the jet or the wake in two or three dimensions. In other words, the dimensionless

velocity profile in the wake of a cylinder or a jet in two or three dimensions at large distances from the origin is independent of the shape of the body that originally generated this vorticity field. This fact is illustrated in this paper with fair certainty. All that has been said in this introductory discussion pertains to the findings of previous investigators such as Schlichting (refs. 1 and 2), Tollmien (refs. 3 and 4), Reichardt (ref. 5), Forthmann (ref. 6), and recently Corrsin (ref. 7) and Townsend (ref. 8), and others. The investigation presented in this paper is primarily concerned with the effects of upstream turbulence level and velocity gradients on the decay of wakes restricted in a channel flow. The upstream conditions ahead of the cylindrical wire producing the wake were chosen to be those of a fully developed turbulent flow in a channel. The conditions of the upstream flow are thus well established, because of the work of Reichardt (refs. 9 and 10) and Laufer (ref. 11). The cylindrical wire was then placed at various locations in the fully developed turbulent shear layer and its process of decay measured until the flow assumed its original fully developed character. This paper contains an analysis based on experimental observations of the mean-velocity decay, static-pressure decay, and turbulence decay behind the cylinder placed in the viscous layer at various distances from the channel walls.

For turbulent wakes and jets any analytical investigation available today is based on a so-called "semiempirical analysis" which makes use of Prandtl's mixing-length hypothesis, Boussinesq's constant-shear-coefficient hypothesis, or Taylor's constant transport of vorticity. Naturally these assumptions become very useful in handling mathematically the additional turbulent terms that appear when turbulent motion is considered. All of these assumptions are in fair agreement with the experimental measurements taken across the wake or jet. The work pertaining to this paper is compared with the analysis for wakes in free-stream turbulent flow.

This investigation was carried out at Syracuse University under the sponsorship and with the financial assistance of the National Advisory Committee for Aeronautics.

SYMBOLS

b_o value of y_w where velocity deficiency is half that of its maximum

c_D drag coefficient of wire computed from momentum change

D diameter of tripping wire, 0.049 in.

d channel width measured locally; d_{av} = 3.856 in.

F(n) power spectrum of turbulence

L decay length until $\Delta U_T = 0.03\ U_s$

L_x	x-component of integral scale
M	time constant of hot wire
n	turbulence frequency
p	local static pressure
p'	turbulent static-pressure fluctuation
Δp	static-pressure drop with reference to wall static pressure
q_s	dynamic pressure corresponding to undisturbed velocity
q'	turbulent dynamic-pressure fluctuation
R_x	x-component of correlation function
U	x-component of temporal mean velocity
U_{av}	space mean velocity
U_o	maximum velocity in undisturbed shear flow
U_s	undisturbed velocity ahead of and at center of disturbance
U_T	total velocity as measured $\sqrt{U^2 + V^2}$, very nearly equal to U
ΔU_T	velocity deficiency in wake, nearly equal to u_1, or deficiency in U
U_∞	free-stream velocity
U_*	shearing velocity, $\sqrt{\tau_\omega/\rho}$
u',v'	instantaneous turbulent velocity fluctuations in x- and y-directions
u_1	velocity perturbation in x-direction
$\tilde{u}'$	root mean square of u'
V	y-component of temporal mean velocity
v_1	velocity perturbation in y-direction
x	Cartesian coordinate along length of channel
y	Cartesian coordinate normal to channel walls
y_w	coordinate from center of wake
η	y-location of axis of tripping wire
ν	kinematic viscosity of air

ξ dimensionless velocity deficiency

ρ density of air

σ ratio of compensated to uncompensated signal from hot wire

τ_w shear stress at wall

Superscript:

$\overline{}$ time average

ANALYTICAL CONSIDERATIONS

The problem under consideration is the turbulent mixing in the wake of an infinite cylinder placed in a two-dimensional fully developed channel turbulent shear layer. The presence of the pressure and velocity gradients together with the comparatively high levels of turbulence makes the exact solution of the problem untractable because of the complicated nature of the flow phenomenon. Attempts are made herein to explain the results obtained through semiempirical hypotheses.

Two-Dimensional Wake in a Laminar Free Stream

Because the decay length of the wake is much larger than its width, many terms in the Navier-Stokes equations become very small compared with others. Far enough downstream of the cylinder the perturbations suggested by Oseen are

$$U = U_\infty + u_1$$

and

$$V = v_1$$

When U_∞, the value of the velocity in the free stream, and u_1, the velocity deficiency in the wake considered negative, are substituted in the Navier-Stokes equations, one obtains a linearized set of equations

$$U_\infty \frac{\partial u_1}{\partial x} = -\frac{1}{\rho}\frac{\partial p}{\partial x} + \nu \frac{\partial^2 u_1}{\partial y^2}$$

$$U_\infty \frac{\partial v_1}{\partial x} = -\frac{1}{\rho}\frac{\partial p}{\partial y} + \nu \frac{\partial^2 v_1}{\partial y^2} \qquad (1)$$

provided U_∞ is a constant and far enough downstream terms like $u_1(\partial u_1/\partial x)$ and $u_1(\partial v_1/\partial x)$ are small compared with the ones in equation (1).

Since the angle of the wake spread is small, the measured values of the longitudinal velocity represent $U_T = \sqrt{U^2 + V^2} \approx U$ and the measured velocity deficiency $\Delta U_T \approx u_1$. For simplicity in the presentation, u_1 is used in the analysis, while the experimental results are shown as ΔU_T.

The continuity equation is

$$\frac{\partial u_1}{\partial x} + \frac{\partial v_1}{\partial y} = 0$$

The general solution to this problem (ref. 12) is in the form

$$\left.\begin{aligned} p &= - U_\infty \frac{\partial \varphi}{\partial x} \\ u_1 &= \frac{\partial \varphi}{\partial x} + \frac{e^{kx}}{2k}\left(\frac{\partial \chi}{\partial x} - k\chi\right) \\ v_1 &= \frac{\partial \varphi}{\partial y} + \frac{e^{kx}}{2k}\frac{\partial \chi}{\partial y} \end{aligned}\right\} \qquad (1a)$$

where $k = U_\infty/2\nu$ and the functions φ and χ satisfy:

$$\nabla^2 \varphi = 0$$

and

$$(\nabla^2 - k^2)\chi = 0$$

The differential equation for χ in u_1 solves in the form

$$\chi = \sum_{n=0}^{\infty} C_n K_n(kr)\cos n\theta$$

where C_n is a constant, K_n is the modified Bessel function, r is the radial distance from the center of the cylinder, and θ is the angular coordinate. For large values of r and small values of θ, which indicate the flow far from the cylinder and inside the wake, one can show in the limiting case that

$$u_1 = \left(\frac{\pi}{2kr}\right)^{1/2} e^{-kr(1 - \cos\theta)} \sum_{n=0}^{\infty} C_n$$

But then for large r and small θ

$$kr(1 - \cos\theta) \approx \frac{1}{2} kx\theta^2 \approx \frac{1}{2} k \frac{y_w^2}{x} \approx \frac{U_\infty y_w^2}{4\nu x}$$

and consequently far downstream the solution takes the form

$$u_1 = C\left(\frac{\pi\nu}{U_\infty x}\right)^{1/2} \exp\left[-\frac{U_\infty (y_w)^2}{4\nu x}\right] \tag{2}$$

It should be noted at this point that in a channel flow with constant pressure gradient equation (1a) and consequently $\nabla^2\varphi = 0$ are not satisfied. The effect on the pressure drop in the channel is discussed later. The solution of equation (2) is the same if one neglects p and v to begin with and solves the parabolic equation

$$U_\infty \frac{\partial u_1}{\partial x} = \nu \frac{\partial^2 u_1}{\partial y^2} \tag{3}$$

The arbitrary constant C must be found from the so-called initial condition and in this case at $x = 0$. If the coordinate system is translated to the center of the wake, and when $y_w = 0$, $u_1 = (u_1)_{max} \sim x^{-1/2}$, then the dimensionless form of velocity deficiency given in equation (2) becomes

$$\xi = \frac{u_1}{(u_1)_{max}} = \exp\left[-\frac{U_\infty (y_w)^2}{4\nu x}\right] \tag{4}$$

Let $y_w = b_o$ where $\xi = 1/2$; then equation (4) becomes

$$\xi = e^{-a\left(\frac{y_w}{b_o}\right)^2} = e^{-a\zeta^2} \tag{5}$$

where $a = 0.6932$, $\zeta = y_w/b_o$, and $b_o = 1.66\sqrt{\nu x}/\sqrt{U_\infty}$. It is surprising to know that experimental data pertaining to laminar and turbulent wakes agree very well with the dimensionless form of equation (5). It is even more surprising to see in figure 27 that equation (5) does not limit itself to wakes alone but describes very well the behavior of laminar or turbulent jet flows.

This extreme similarity in the laminar and turbulent mixing is what led Reichardt (ref. 13) to believe that there should be a universal law for the free mixing of any type of velocity discontinuity set up in the free stream. What is most fortunate for this investigation is that, despite the difficulties introduced by the turbulent fully developed shear

layer and the pressure drop, figure 7 shows still a remarkable agreement with equation (5) derived for laminar flow in the free stream. The experimental results in figure 7 were extended purposely on both sides of the wake in order to examine the effects of the asymmetry in the boundary conditions. It should be noted here that for positions of the cylindrical wire $0.20 < \eta/d < 0.50$ investigated in this work the dimensionless experimental results correlate well, as shown in figure 7. A general statement for the entire boundary layer should not yet be inferred. For positions $0 < \eta/d < 0.20$, where turbulent agitations and energy transports become extremely large, the behavior of the wake is intuitively expected to be different. Also in this region very near the channel wall, the presence of the wall on one side of the wake will limit greatly the transport of energy and momentum. The experimental results in figure 6 for $\eta/d = 0.0715$ substantiate this fact. Another important point to remember at this stage is that equation (5) does not explicitly determine the dependence of u_1 on x and y_w, except for the laminar free-stream case solved. Schlichting (ref. 14) tabulates the dependence of u_1 and b_o on x for various experimentally investigated free-mixing problems. The dependence of u_1 and b_o pertaining to this work is established experimentally in figures 24 and 25.

Wakes in Pressure Gradients

Since Goertler (ref. 15) has shown that, with the assumption of a constant shear coefficient in the wake, the turbulent wake in the free stream reduces to the same problem as that of the laminar wake with the exception that the kinematic viscosity ν is replaced by a "virtual kinematic viscosity" which includes the effects of the turbulent shear stresses, the influence of the turbulence level on the dimensionless solution (5) is neglected here. Since the diameter of the wire D is approximately 0.02 d, it is assumed for the ranges of η/d investigated that U is an average value of the undisturbed flow just outside the wake. Then modifying equation (3) by including the constant pressure gradient yields

$$\partial p/\partial x = -A$$

$$\frac{\partial^2 u_1}{\partial y^2} - \frac{U_\infty}{\nu}\frac{\partial u_1}{\partial x} + \frac{A}{\rho\nu} = 0 \qquad (6)$$

This equation is similar to the one-dimensional unsteady-state heat conduction equation for constant heat generation. Two simple transformations can reduce equation (6) to the form of equation (3), which can be solved readily. The two transformations are $u_1 = \varphi + (A/\rho U_\infty)x$ and $u_1 = \varphi - (A/2\rho\nu)y^2$. Upon substitution equation (6) takes the form of equation (3) in φ. Because of these substitutions, some difficulties do arise when satisfying the boundary conditions. The first transformation is not adequate, since u_1 grows with x. The second transformation

also gives difficulties when y is very large, but if one assumes that the wake has a finite width b where $\varphi - (A/2\rho\nu)b^2 = 0$ and consequently neglects the outer region, the problem reduces to the previous solution from equation (3) minus a parabolic term in y. The influence of the pressure gradient is then felt on the outer regions of the wake depending on the value of A (see following sketch). Behind the wire and in the near vicinity of it,

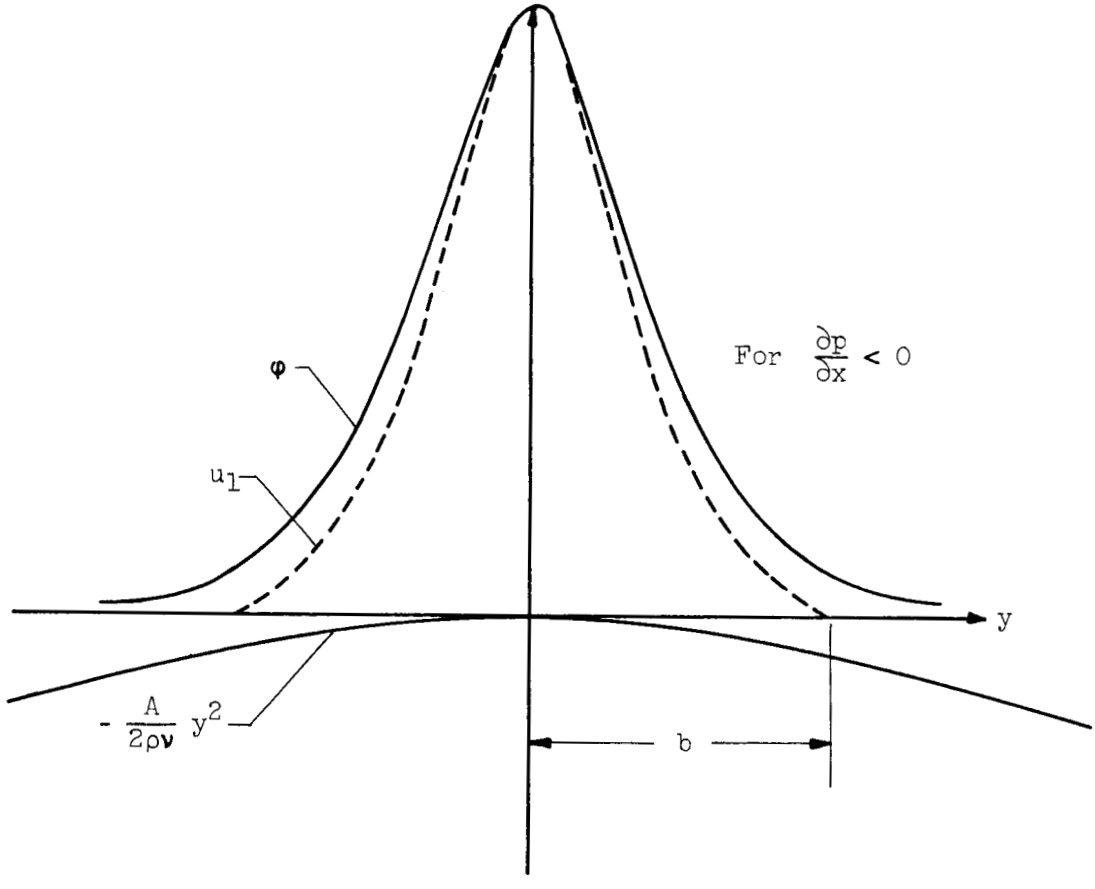

$\partial p/\partial x > 0$ for the viscous wake and is usually much larger than A, and consequently the effect then is to increase the values of u_1 toward the edges of the wake. From figure 7 this observation can be for values of x/D less than the equilibrium region of the wake or jets. As long as $\partial p/\partial x$ is mild, its effects can be neglected. From figure 7 and from comparison of data pertaining to viscous wakes in the vicinity and far away from the cylinder one can conclude that the pressure gradient must be quite large to distinguish its effects from experimental errors.

General Considerations

Since experimental results show that the dimensionless analytical form of the mean-velocity deficiency given in equation (5) is in good agreement with wakes in a flow field with zero or finite mean vorticity, with low or relatively high levels of turbulence one may consider the relation as universal. The material in the appendix extends this universality to two-dimensional and round jets. Since relation (5), as already mentioned, does not state explicitly the dependence of $(u_1)_{max}$ and b_o on x, for lack of an exact turbulent solution $(u_1)_{max}$ and b_o must be determined experimentally so that u_1 or approximately ΔU_T is known as a function of x and y. Schlichting (ref. 14) gives from experiments these functions in tabulated form for the free mixing of jets and wakes. Naturally owing to the relatively high turbulence level, vorticity, pressure gradient, and restricted motion, the x-dependence of ΔU_T and b_o differs in the shear layer from those already tabulated by Schlichting. These functions are represented in figures 24 and 25. The dependence of b_o on x/D seems to be the same for all $0.2 < \eta/d < 0.5$, while the dependence of $(u_1)_{max} \approx (\Delta U_T)_{max}$ shows a slight trend of faster decay for smaller values of η/d.

EXPERIMENTAL EQUIPMENT AND PROCEDURES

Wind Tunnel

The experimental results were obtained in the wind tunnel at Syracuse University designed especially for this investigation. A side view of the tunnel is shown in figure 1. On this figure, after the nozzle, the partition 0.064 by 60 by 144 inches does not apply to this work and consequently should not mislead the reader. For two-dimensionality, the internal cross section of the channel has an aspect ratio of 14.5. The channel wall sections are made of 3/4-inch by 5-foot by 10-foot birch veneered plywood. Dry and treated maple ribs $1\frac{1}{2}$ by 2 by 60 inches were glued under pressure behind the plywood sheet at 12-inch intervals. Finally, on a flat table, under pressure, a sheet of 1/4-inch by 5-foot by 10-foot plywood was screwed on the ribs. This backing sheet ensured additional stiffening. The end ribs of each section were wider maple ribs, predrilled for doweling and machined before they were cut in half. This process ensured excellent matching when two sections were joined together. The static-pressure taps and the probing stations were made of bronze cylindrical inserts originally ground perpendicular to the axis of the cylinder. The holes on the walls to receive these inserts were drilled with a precision machine-shop drill resting on the surface of the plywood itself (see fig. 2). The walls were coated with a moisture sealer

and furniture wax. The top and bottom channel spacers were made of aluminum channels machined for square sides and uniform width.

Tripping Wire and Its Mechanism

The diameter of the tripping wire was chosen such that its Reynolds number, based on the lowest velocity at the wire position in the shear layer, was larger than the upper limit of the periodic vortex formation. The upper limit on the diameter of the wire was governed by its blocking area in the channel $\left(\text{less than } 1\frac{1}{2} \text{ percent}\right)$. The diameter of the wire used for this investigation was 0.049 inch, which gave a blocking ratio of $1\frac{1}{4}$ percent. This ratio is small enough so that its effects can be neglected. The piano wire was held through the channel with some tension by two lathe slide rests mounted on the top and bottom of the channel. The slide rest had two lead screws with graduated collars that provided accurate longitudinal and transverse motion of the wire in the shear layer. Before any measurement, the wire was brought in contact with the probe and then moved back to the desired position.

Probe Traversing Mechanism

For measurements across the viscous layer and the wake, a traversing mechanism similar to the one shown in figure 2 with an additional positive displacement dial indicator was used. The accuracy of the probe displacement was better than 0.001 inch.

Total- and Static-Pressure Probes

The total-pressure probes were made of small brass tubing flattened at the sensing end to an opening of 0.005 inch. The walls of the flattened tube were then ground to 0.007 inch. Since measurements were not performed at a distance less than $x/D = 5.1$, where the width of the wake was 0.25 inch, the opening of the total-pressure probe was approximately one-fiftieth the width of the wake. These proportions ensured accurate total-pressure measurements in regions with moderately high velocity gradients. The static-pressure probes were made with 0.024-inch-outside-diameter tubing filed smooth at the end and with only two holes drilled along the axis of the tripping wire. Without the tripping wire, the static pressure across the channel, except in the immediate vicinity of the walls, was very nearly equal to the value at the walls. In any case, the calibration of the probe in the channel without the tripping wire was considered, even though it was small compared with the static-pressure distribution behind the wire. In all cases, the stem of the probe produced

a small shift in the axis of the wake. This small shift remained almost constant throughout the experiments, and it is discussed later.

Hot-Wire Equipment

The hot-wire equipment was of the constant current type. The set was designed and built at Syracuse University and was similar to the set mentioned in reference 16. The wires used were tungsten, 0.00015 inch in diameter, and displayed a time constant of approximately 1.0 millisecond. The compensation of the wire delay was good up to 15 kilocycles. The hot wire was copper plated and mounted on long, thin jeweler broaches to reduce the influence of the probe on the flow.

EXPERIMENTAL RESULTS

Preliminary Measurements Without Tripping Wire

Since the object of this work is to analyze the decay phenomenon of a wake in a turbulent viscous layer, a fully developed viscous layer was chosen for the initial conditions of the flow. There are two essential reasons for this choice. The first consideration was that this type of flow has been thoroughly investigated, and consequently its properties are well known. The second and most important consideration was that no further development of the flow itself (without the tripping wire) could be tolerated if the effects of the cylindrical disturbance alone were to be analyzed. Figure 3 shows the static-pressure drop along the channel without the presence of the wire. The approximate location of the tripping wire is shown. The percent width variation through the entire channel is also shown, together with the correlating evidence of the departure from linear static-pressure drop due to width variations. Considering the channel width, the width variations are well within expected tolerances for wood construction. An estimate was made of the daily variations of the widths due to changes in atmospheric conditions. The maximum value observed was 1/2 percent. Upstream of the tripping wire, the mean-velocity distribution and turbulence intensity showed the flow had reached the fully developed state. Figure 4 shows the logarithmic form of the mean-velocity distribution at two longitudinal stations in the neighborhood of the wire location. Furthermore, in figure 5(a) the lower curve represents the velocity profile upstream of the tripping wire and at the end of the decay process.

Figure 4 also shows that the viscous layer in this work falls between that reported by Laufer (ref. 11) for his channel and the generally accepted law for the flat-plate boundary layer without pressure gradient.

The value of the intercept of the logarithmic law for this work and that of Laufer are almost the same. This is not a coincidence, since in both cases the wind-tunnel walls were made of birch plywood and their surface was treated in the same fashion. The slopes of the curves are different, and a survey of the literature showed that the slope depends on the level of the pressure gradient.

The Reynolds number of the channel based on the space mean velocity and half the channel width is 86,000. The shear stress at the wall computed from the pressure drop is

$$\frac{\tau_w}{\rho U_o^2} = 0.0014$$

This value was also verified from measurements of the mean velocity in the sublayer obtained with the hot-wire anemometer. Measurements also showed that the flow was two-dimensional within the accuracy of measurements.

Space Mean Velocities in Wake

Mean-velocity measurements were taken at six positions in the shear layer, namely, at values of η/d of 0.0715, 0.20, 0.29, 0.35, 0.40, and 0.496. Longitudinal distances behind the wire for each transverse position ranged for values of x/D shown in figure 5. As seen from the figures, two methods were used to make the measured velocities dimensionless. The quantities shown in figure 5(a) are compared with the spacial mean velocity for the reason that at certain locations of the wire the maximum velocity in the shear layer fell inside the wake. This method, although adequate, involved space integration of the velocity profiles. The second method, just as adequate, consisted of successive measurements in the wake and corresponding measurements 60 to 120 diameters upstream of the wire. The advantage of this method over the first one was that corresponding measurements at equal y/d's upstream and in the wake were taken consecutively. Scatter in the deficiencies of the velocities was somewhat reduced. The value of U_o in figures 5(b) and (c) refers to the maximum velocity upstream of the wire. As mentioned by Kovasznay (ref. 17), the stem of the probe caused a slight shift of the center of the wake in a direction away from the side of the stem. This shift was consistent at all η/d values, including the center of the channel. The shift was largest in the vicinity of the wire and decreased very fast downstream, approximately $(1/2)D$ at a distance $10D$ downstream and a little less than $2D$ at about $x/D = 240$. The distributions of the mean velocity in the wake shown in figure 6 were corrected for this shift. At first this was considered the effect of circulation around the wire due to an undisturbed flow with a velocity gradient. Calculations of that effect showed it to be much smaller than the measured shift of the center of the wake. The velocity deficiency in the wake is plotted in figure 6

as a ratio to the undisturbed velocity at the center and upstream of the wire U_S. In this form the process can be compared with that of a free-stream flow.

For the choice of $D/d = 0.0127$ selected, it was found that in the regions $0.20 < \eta/d < 0.50$, for half the channel flow, the wake completely disappears before one side reaches the wall. This region is analyzed here in more detail. When $\eta/d < 0.20$, as shown for instance in figure 6 for $\eta/d = 0.0715$, one side of the wake soon spreads to the wall, and its mixing process is completely altered, since because of the presence of the solid boundary the wake received very little energy transport from the surroundings at that side as compared with its free side. Consequently, the entire mixing process suddenly becomes much slower. From this time on this process was excluded from the subsequent analysis, not because of a lack of interest, but because it introduces the additional effects of the parameter D/d. When this decay process is plotted as in figure 24, it starts in the same fashion as the other curves but later remains almost parallel to the case of Townsend.

Looking at the velocity distributions in figure 5, except for the center of the channel, the distribution of the velocity in the wake is not symmetrical with respect to the direction of flow. However, when velocity deficiencies are calculated from the values of the velocities with and without the wake at the same y/d, the distribution of ΔU_T becomes symmetrical for the major portion of the wake except at the edges, where the end conditions have different turbulent properties. This fact is shown in figure 7, and it pertains to all $0.20 < \eta/d < 0.50$. As mentioned in the analysis, the dimensionless form of the velocity deficiencies agrees very well with the analysis based on laminar flow or that of turbulent flow in a free stream with the assumption of a constant shear-stress coefficient. Accepting the relation

$$\frac{\Delta U_T}{(\Delta U_T)_{max}} = \exp\left[-0.6932\left(\frac{y_w}{b_o}\right)^2\right] \tag{5a}$$

to be valid also for this type wake, provided the wake never spreads to the wall, it becomes a problem to establish the dependence of $(\Delta U_T)_{max}$ and b_o on the coordinate x. The problem for the mean-velocity distribution is then solved semianalytically for values of $0.20 < \eta/d < 0.50$ or for $\eta/D > 15.7$.

Static Pressure in Wake

Static-pressure distributions in the vicinity of the cylinder were measured, and a typical distribution is shown in figure 8. The term Δp

is the pressure drop caused by the viscous wake. The measurements show that the changes in static pressure caused by the cylinder disappear to 1 percent of the dynamic pressure at a distance of 30D. Since for the position of the wire $\eta/d = 0.0715$ the wake has not spread to the wall at $x/D = 25.5$, the decay of the static-pressure peak is also represented in figure 9. It could be noticed in figure 8 that very near the wire, at $x/D = 5.1$, the static-pressure deficiency has an increase outside the wake for a small y/d distance. This is attributed to the potential effects of the flow in the vicinity of the wire.

Turbulence Measurements

Turbulence intensities. - The root-mean-square values of the turbulence in the direction of the flow were measured at various distances downstream of the tripping wire. In order to compare the influence of the shear-layer properties on the decay, the tripping wire was placed at four transverse locations: $\eta/d = 0.072$, 0.20, 0.292, and 0.50. The local turbulence levels are presented in figures 10 to 13. From these figures it is apparent that the level of turbulence generated at the start of the wake behind the tripping cylinder is not a function of which portion of the shear layer was tripped. In other words, it can be said that, for varying trip positions, the turbulence generated in the proximate vicinity of the tripping wire is the same, but the absolute rate of decay is different at different locations of the tripping wire. Figure 14 shows the decay of turbulence intensity at the center of the wake for various locations of the trip position. It is interesting to note that the turbulence decay at the center of the shear layer extends very nicely into Townsend's data taken in a free stream with low turbulence (ref. 8).

A comparison of the total decay rate should not be derived from the slope of these curves alone, because the end conditions at the different tripping-wire locations are not the same. For instance, at $\eta/d = 0.072$, the decay will be completed at a level of approximately $\tilde{u}'/U = 0.095$, while at $\eta/d = 0.5$ the decay will go down to a level of $\tilde{u}'/U = 0.038$. The representation of total amount of turbulence to undergo decay is shown in figure 15. This figure indicates the amount of turbulence at the center of the wake above the initial or final state in the shear layer. Since Townsend's initial turbulence is zero, his curve remains as in figure 14. These curves show the same rate of decay on all four trip positions. The only difference among them is that the origin is lower for trip positions near the solid boundary. This is due to the fact that the final level of turbulence is larger near the solid boundary. For comparison of decay lengths, figure 16 has been drawn from the data in figure 15. An arbitrary level of turbulence $\Delta\left(\frac{\tilde{u}'}{U_{max}}\right) = 0.25$ was chosen above the final state, and the length of process to reach that level is plotted in figure 16 as a function of the trip position η/d. At the

arbitrarily chosen level, it becomes apparent that it takes twice the length at $\eta/d = 0.072$ than at the center of the channel.

Up to this point comparisons have been made of the absolute and relative orders of magnitude of the turbulence level of the center of the wake as it decayed downstream from the tripping cylinder. A comparison of the proportionate levels with respect to the final state is presented in figure 17. Here the values presented in figure 15 are divided by the level of turbulence when the decay process is completed or by the initial level of turbulence.

Integral scales. - If one assumes that the power spectrum of turbulence intensity in the main direction of flow can be empirically represented by (ref. 11)

$$F(n) = \frac{2}{\pi} \frac{L_x/U_o}{1 + n^2 L_x^2/U_o^2} \tag{7}$$

then it is possible to show (ref. 18) that the integral scale L_x can be obtained from the ratio of the compensated to uncompensated turbulent energies. This expression turns out to be:

$$L_x = \frac{MU_o}{\sigma - 1} \tag{8}$$

where M is the time constant of the wire, U_o is the maximum velocity in the shear layer, and σ is the ratio $(\overline{u'^2})_{comp}/(\overline{u'^2})_{uncomp}$. This relation for L_x was shown by Laufer (ref. 11) to approximate fairly well the integral scale in the fully developed turbulent shear layer as defined from the integral of the correlation function

$$L_x = \int_0^\infty R_x \, dx \tag{9}$$

where R_x is the correlation coefficient of two turbulent signals along the direction of flow separated by a distance x.

Power spectra measurements were not taken, and consequently the validity of equation (7) for the power spectrum in the wake was not invesgitated. However, in figure 18 the increase in L_x/D with distance downstream from the wire shows that, at the center of the wake, the process originates at approximately $L_x/D = 1.0$, which shows good reliability in the method.

The time constant M was determined from the compensating electrical network. The distribution of L_x across the wake at different locations of the tripping cylinder is presented in figures 19 to 22. As mentioned above, the levels of L_x at the center of the wake as a function of distance downstream are shown in figure 18 for various positions of the tripping wire.

Comparison of these scales with those of Townsend performed in the free stream is not possible, since the ultimate final state of the scales in a free-stream wake is different from that in the fully developed turbulent shear flow.

The integral scale is one measure of the turbulence structure. The pattern of the turbulence fluctuation u' was photographed from the oscilloscope. Figure 23 demonstrates the difference in structure between a point at the center of the wake and one just outside the wake. The time scales on the pictures are the same. The pattern just outside the wake was taken in order to see whether intermittency of turbulence efflux at the wake boundaries could be noticed. Patches of high frequency can be observed in the lower trace. The measured values of the integral scales also show the abundance of high frequency (low scales) at the center of the wake when compared with that outside the wake.

Decay Phenomenon of Velocity Deficiency

If equation (5a) is considered a representative dimensionless velocity-deficiency distribution in the wakes in turbulent shear flows for $0.20 < \eta/d < 0.50$ and $\eta/D > 15.7$, then establishing the dependence of $(\Delta U_T)_{max}$ and b_o as a function of x establishes the mean-velocity distribution in the wake. The variations of $(\Delta U_T)_{max}/U_s$ for various positions η/d are shown in figure 24 (U_s is the undisturbed velocity at the center of the wire, that is, at η/d). The velocity deficiency does not decay with a simple power law as in the case of the free stream, as shown by Townsend's measurements on the same figure. One could even argue about the linearity of Townsend's results and make his experimental points fall on a curve with the same origin and belonging to the family of curves shown. Townsend (ref. 8) has already shown in his analysis of turbulent wakes in the free stream that, if similarity exists in the mean-velocity distribution and the turbulent shear stress, and also if the similarity law of the mean velocity is assumed to be a Gaussian error function, then from the momentum and energy equation the decay of the maximum velocity deficiency is somewhat different from the simple power law of -1/2. His expression was in the form

$$\frac{(\Delta U_T)_{max}}{U_s} = \frac{1}{\sqrt{\frac{x}{D} + B\left(\frac{x}{D}\right)^{1/2}}}$$

For this case B was determined to be 0.43. Actually the process of decay here is much faster, since for large values of x/D the curves in figure 24 take an average slope of about -4/5. In this investigation it is expected that the decay process should be faster than that of a wake in a free stream. This is easily explained by observing the terms in the equation for the rate of turbulent energy interchange:

$$\frac{1}{2}\left(U\frac{\partial}{\partial x}\overline{q'^2} + V\frac{\partial}{\partial y}\overline{q'^2}\right) + \frac{1}{2}\left(\frac{\partial}{\partial x}\overline{u'q'^2} + \frac{\partial}{\partial y}\overline{v'q'^2}\right) + \left(\overline{u'^2}\frac{\partial U}{\partial x} + \overline{u'v'}\frac{\partial U}{\partial y}\right)$$

$$= -\frac{1}{\rho}\left(\frac{\partial}{\partial x}\overline{p'u'} + \frac{\partial}{\partial y}\overline{p'v'}\right) + \nu\left(\overline{u'\nabla^2 u'} + \overline{v'\nabla^2 v'}\right) \qquad (10)$$

In the vicinity of the wire, where gradients in the x- and y-directions are large, the entire equation (10) applies. In the region far downstream of the wire the terms involving gradients in x may be neglected compared with those in y and equation (10) becomes

$$\frac{1}{2}\left(U\frac{\partial}{\partial x}\overline{q'^2}\right) + \frac{1}{2}\left(\frac{\partial}{\partial y}\overline{v'q'^2}\right) + \left(\overline{u'v'}\frac{\partial U}{\partial y}\right) = -\frac{1}{\rho}\left(\frac{\partial}{\partial y}\overline{p'v'}\right) + \left(\overline{u'\nabla^2 u'} + \overline{v'\nabla^2 v'}\right) \qquad (10a)$$

The energy transport inside the wake due to the order of magnitude of the terms above is helped considerably by the gradients outside the wake as well. The first quantity in parentheses in equations (10) and (10a) indicates the rate of energy convected by the mean flow. The second parentheses represents the diffusion of turbulent energy by the turbulent motion. The third is the production of turbulent energy, the fourth is the work due to the pressure fluctuation, and the last includes the viscous dissipation and viscous work. It is interesting to note that the end of the wake on the wall side of the shear layer has a much greater influence because of its larger gradients than the other side of the wake. This is the reason the conditions at the two ends of the wake as shown in figure 7 are not identical. In the case of $\eta/D < 15.7$, when the edge

of the wake reaches the wall, the energy interchange with the outside is limited to the outer side of the wake, and consequently the decay process is slower.

Spread of Wake

The spread of the wake represented in figure 25 does not seem to be a function of the position of the tripping wire as the maximum velocity deficiency does. The spread of b_o is again faster than that obtained by Reichardt (ref. 5) and Schlichting (ref. 2) for a free-stream two-dimensional wake. Since the momentum in the wake is related to the drag on the cylinder, by integrating over a control surface enclosing the cylinder, the drag and consequently the drag coefficient were calculated and entered in the dimensionless representation of the spread b_o in figure 25. The spread of the wake can then be represented for all η/d by a simple power law with an exponent 0.59.

Scale of Decay for Mean Velocity

In order to establish a relative order of magnitude of the length x/D, the wake must decay at various locations η/d of the cylinder; an arbitrary decay of the wake corresponding to $(\Delta U_T)_{max}/U_s = 0.03$ was chosen for comparison. If in figure 24 a line is drawn through the value of the ordinate 0.03 parallel to the abscissa, the decay lengths L/D are obtained and can be plotted as in figure 26. This figure in linear coordinates shows the influence of η/d on the decay phenomenon better than the logarithmic representation in figure 24. The free-stream decay of the wake to the 3-percent value of the undisturbed velocity ahead of the cylinder would have taken approximately 950D, as shown in figure 24. This indicated that the decay process in the shear layer is at least three times as fast as the one in the free stream. This shortening of the decay length is due to:

(1) The high levels of turbulence at the origin of the wake

(2) The spread of the wake into a turbulent and relatively high vorticity field where turbulent energy is transported in the absence of the wake

(3) The presence of the favorable pressure gradient in the channel which accelerates the motion in the wake

CONCLUSIONS

The experimental measurements in the wake of a two-dimensional cylinder in a fully developed turbulent viscous layer showed the following points of interest:

1. The dimensionless mean-velocity deficiency in the wake displays similarities with the laminar or turbulent wake in a free stream. The asymmetry of the conditions of the flow outside the wake makes itself felt at the edges of the wake.

2. The effect of the favorable pressure drop in the wind tunnel is to help reduce the velocity deficiency throughout the wake. The pressure drop was not large enough to affect the similarity.

3. For the ratio of cylinder diameter to channel width in this experiment, when the cylinder is placed at a distance from the wall smaller than $\eta/d = 0.2$, the wake spreads to the wall before being completely mixed (η, distance of tripping wire from channel wall; d, local channel width). The process of mixing becomes much slower after one edge of the wake has spread to the wall.

4. The static-pressure gradients due to the cylinder and in the vicinity of the cylinder can be completely neglected after 30 cylinder diameters.

5. When the cylinder is at the center of the channel, the longitudinal decay of the velocity deficiency requires a length three times as short as the decay in the free stream. When the cylinder is at a distance from the wall $\eta/d = 0.2$, the decay length is reduced by a factor of four when compared with the free-mixing problem with a low-turbulence free stream.

For the region in the viscous layer where the cylinder was positioned $0.2 < \eta/d < 0.5$, the mean-velocity gradients and the turbulence level in the undistributed flow do not vary considerably. It would be of interest to choose a smaller ratio of wire diameter to channel width D/d and approach the wall even further, making sure the wake decays to a reasonably low value before it spreads to the wall. Also it would be of interest to study the decay process when one edge of the wake spreads to the wall.

Syracuse University,
Syracuse, N. Y., January 7, 1959

APPENDIX - DISCUSSION ON WAKES AND JETS IN UNIFORM FREE STREAMS

The problem of free mixing of two- or three-dimensional jets and wakes shows remarkable similarities, far enough downstream, in the distribution of the mean velocity. This fact was mentioned by Reichardt (ref. 13) and led him to believe that all free-mixing processes of velocity discontinuities reach a condition far enough downstream where the process could be described by the one-dimensional heat equation with nonconstant coefficients. This work is referred to in the literature today as the inductive theory of turbulence.

This amazing similarity in the free-mixing processes is shown here in some detail for the reason that it not only applies to free-stream conditions that are uniform but to free streams with moderately high vorticity and turbulence as well, as in the case of this investigation.

The dynamic equations for the mean motion of the flow far enough downstream of a cylinder reads as equation (1) or (3). U_∞ is the free-stream velocity, u_1 and v_1 are the components of the velocity deficiency. The solution of these equations is given in equation (4) and in a more general form in equation (5). Since the experimental data for the laminar as well as the turbulent wake agree well with equation (2) and consequently equation (5),

$$u_1 = Cx^{-1/2} \exp\left[-\frac{U_\infty (y_w)^2}{4\nu x}\right] \tag{2}$$

$$\xi = e^{-a\zeta^2} \tag{5}$$

it becomes reasonable to assume that the differential equation for the laminar case (eq. (3)) is also the equation for the turbulent wake except for the coefficients. Goertler (ref. 15) using Prandtl's hypothesis for constant shear coefficient factored the turbulent shear stress with the laminar one and changed the kinematic viscosity into a "virtual kinematic viscosity" ε. The equation pertaining to the turbulent wake is then

$$U_\infty \frac{\partial u_1}{\partial x} = \varepsilon \frac{\partial^2 u_1}{\partial y^2}$$

This implies that the turbulent shear stress is proportional to the laminar shear. The proportionality factor is taken as a constant. Regardless of the coefficients, the dimensionless solution given in equation (5) always satisfies. For $a = 0.6932$

$$\xi = \frac{u_1}{(u_1)_{max}} = e^{-a\left(\frac{y_w}{b_o}\right)^2} = e^{-a\zeta^2}$$

Depending on the type of free mixing, b_o and $(u_1)_{max}$ or $(\Delta U_T)_{max}$ will assume different dependences on x. However, the experimental measurements in figures 27 and 7 show that the dimensionless form in ξ applies to all. The experimental data for two-dimensional jets and wakes and round jets are shown in figure 27 together with the solution of equation (5). Miss Swain (ref. 19) has analyzed the problem of the three-dimensional wake and predicted the same type of solution found by Schlichting for the two-dimensional turbulent wake based on Prandtl's mixing-length theory. Figure 27 shows first that the experimental data pertaining to the different types of mixing correlate remarkably well within the experimental scatter of any one set of measurements. Equation (5a) is a good representative for all the measurements. Figure 28 shows the same experimental points plotted with various analytical solutions derived for each individual case. It can be seen that the analytical solutions show a much wider scatter among themselves than the experimental points pertaining to the different physical configurations.

The various theoretical curves shown in figure 28 should be recognized as follows: Curve 1 is from Schlichting (refs. 2 and 14) assuming constant mixing length across the two-dimensional turbulent free wake according to the equation

$$\frac{\Delta U_T}{(\Delta U_T)_{max}} \approx \frac{u_1}{(u_1)_{max}} = 1 - 0.586\left(\frac{y_w}{b_o}\right)^{3/2} + 0.086\left(\frac{y_w}{b_o}\right)^3$$

The difficulty with this solution is that it gives a finite width for the wake as the solution runs away for large values of y_w. Also, in the center there is a discontinuity in the curvature of the velocity profile.

Curve 2 is equation (2) changed to the form of equation (5) following Goertler assuming a constant shear-stress coefficient in the two-dimensional turbulent wake.

Curve 3 is for the two-dimensional jet of Tollmien (ref. 4). His solution is based on Prandtl's mixing-length hypothesis. The form of the solution is not reported, as it does not appear in a closed explicit form.

Curve 4 is again for the two-dimensional turbulent jet of Goertler (ref. 15), who assumed a constant shear-stress coefficient. In the coordinates of figure 28, his solution transforms into

$$\frac{U_T}{(U_T)_{max}} \approx \frac{u_1}{(u_1)_{max}} = 1 - \tanh^2\left(\frac{0.885\ y_w}{b_o}\right)$$

Curve 5 is Tollmien's solution for the round jet with the same mixing-length assumption he adopted for the two-dimensional jet in his analysis for curve 3. Again the solution is not reported because it does not appear in a closed explicit form.

Curve 6 corresponds to the round jet assuming Goertler's constant virtual kinematic viscosity and a constant jet strength during the expansion

$$\frac{U_T}{(U_T)_{max}} \approx \frac{u_1}{(u_1)_{max}} = \frac{1}{\left[1 + 0.414\left(\frac{y_w}{b_o}\right)^2\right]^2}$$

Miss Swain (ref. 19) has shown that, for a wake behind a body of revolution, the solution reduces to that given by Schlichting for the two-dimensional wake. Corrsin (ref. 7) has shown that using Taylor's assumption of constant transport of vorticity, at least for the round jet, does not give a better fitting solution than those obtained by Prandtl's momentum transfer or constant-shear-coefficient hypothesis. Just from inspection of figures 27 and 28 it becomes apparent that the exponential form of solution (curve 2) seems to represent the experimental values better than the others. The mixing problem of velocity discontinuities created by jets and wakes can be considered with good approximation to be as given by equation (5) where $(\Delta U_T)_{max} = f(x)$ and $b_o = \varphi(x)$ must be determined experimentally.

In general one may say that the general form of mixing solution

$$u_1 = f(x)e^{-a\left[\frac{y}{\varphi(x)}\right]^2}$$

with $u_1/f(x) = \xi$ and $y/\varphi(x) = \zeta$ satisfies the differential equations

$$\xi'' + 2a\xi'\zeta + 2a\xi = 0$$

In the case of the circular jet and two-dimensional wake $f(x) \sim 1/\varphi(x)$.

The functions $f(x)$ and $\varphi(x)$ have been determined experimentally in this work for the decay process of wakes in turbulent shear flow. These functions are represented in figures 24 and 25.

REFERENCES

1. Schlichting, H.: Laminare Strahlausbreitung. Z.A.M.M., Bd. 13, Heft 4, Aug. 1933, pp. 260-263.

2. Schlichting, H.: Über das ebene Windschattenproblem. Ing. Arch., Bd. 1, Heft 5, 1930, pp. 537-571.

3. Tollmien, W.: Grenzschichttheorie. Handbuch der Experimentalphysik, Bd. 4, Teil 1, 1931, pp. 241-285.

4. Tollmien, Walter: Calculation of Turbulent Expansion Processes. NACA TM 1085, 1945.

5. Reichardt, H.: Gesetzmasigkeitein der frein Turbulenz. Forsch. Gebiete Ingenieurw., Ausgabe B, Bd. 13, Forsch. 414, May-June 1942.

6. Förthmann, E.: Turbulent Jet Expansion. NACA TM 789, 1936.

7. Corrsin, Stanley: Investigation of Flow in an Axially Symmetrical Heated Jet of Air. NACA WR W-94, 1943. (Supersedes NACA ACR 3L23.)

8. Townsend, A. A.: The Structure of Turbulent Shear Flow. Cambridge Univ. Press, 1956.

9. Reichardt, H.: Die quadratischen Mittelwerte der Längsschwankungen in der turbulenten Kanalströmung. Z.A.M.M., Bd. 13, Heft 3, June 1933, pp. 177-182.

10. Reichardt, H.: Vorträge aus dem Gebiet der Aero- und Hydrodynamik. Über das Messen turbulenter Längs- und Querschwankungen. Z.A.M.M., Bd. 18, Heft 6, Dec. 1938, pp. 358-361.

11. Laufer, John: Investigation of Turbulent Flow in a Two-Dimensional Channel. NACA Rep. 1053, 1951. (Supersedes NACA TN 2123.)

12. Goldstein, S., ed.: Modern Developments in Fluid Dynamics. Vol. II. Clarendon Press (Oxford), 1938, p. 574.

13. Reichardt, H.: Über eine neuse Theorie der freinen Turbulenz. Z.A.M.M., Bd. 21, Heft 5, Oct. 1941, pp. 257-264.

14. Schlichting, Hermann: Boundary Layer Theory. McGraw-Hill Book Co., Inc., 1955.

15. Göertler, H.: Berechung von Aufgaben der freien Turbulenz auf Grund eines neuen Näherungsansatzes. Z.A.M.M., Bd. 22, Heft 5, Oct. 1942, pp. 244-254.

16. Eskinazi, Salamon, and Yeh, Hsuan: An Investigation on Fully Developed Turbulent Flow in a Curved Channel. Jour. Aero. Sci., vol. 25, no. 1, Jan. 1956, pp. 23-34.

17. Kovásznay, L. S. G.: Hot-Wire Investigation of the Wake Behind Cylinders at Low Reynolds Numbers. Proc. Roy. Soc. (London), ser. A, vol. 198, no. A1053, Aug. 15, 1949, pp. 174-190.

18. Dryden, H. L.: Turbulence Investigation at the National Bureau of Standards. Proc. Fifth Int. Cong. Appl. Mech., John Wiley & Sons, Inc., 1939.

19. Swain, L. M.: On the Turbulent Wake Behind a Body of Revolution. Proc. Roy. Soc. (London), ser. A, vol. 125, no. 799, Nov. 1, 1929, pp. 647-659.

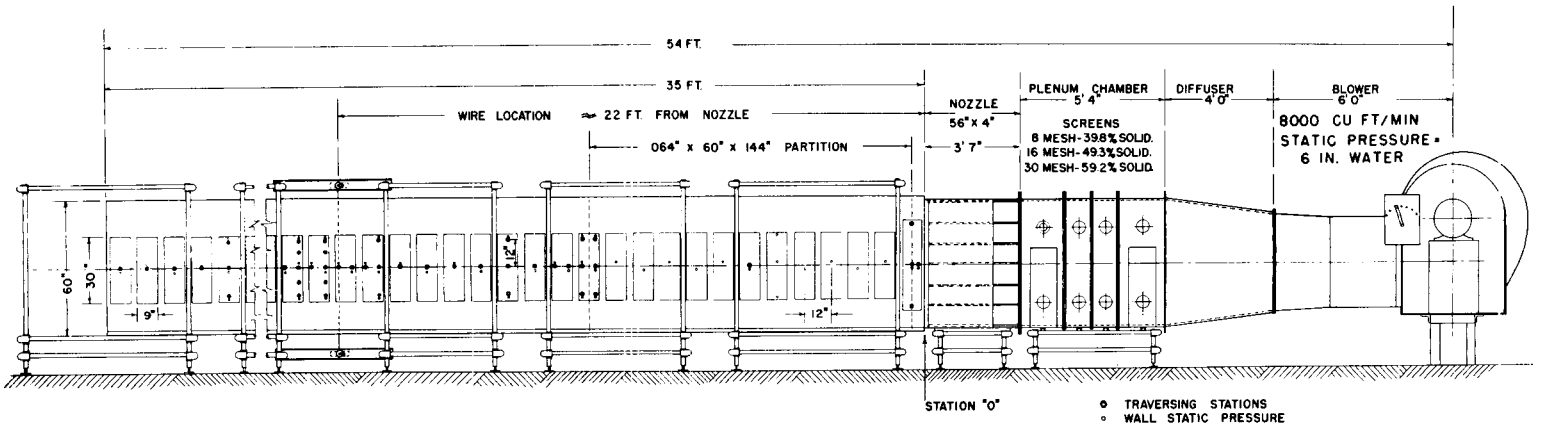

Figure 1. - Side view of wind-tunnel assembly.

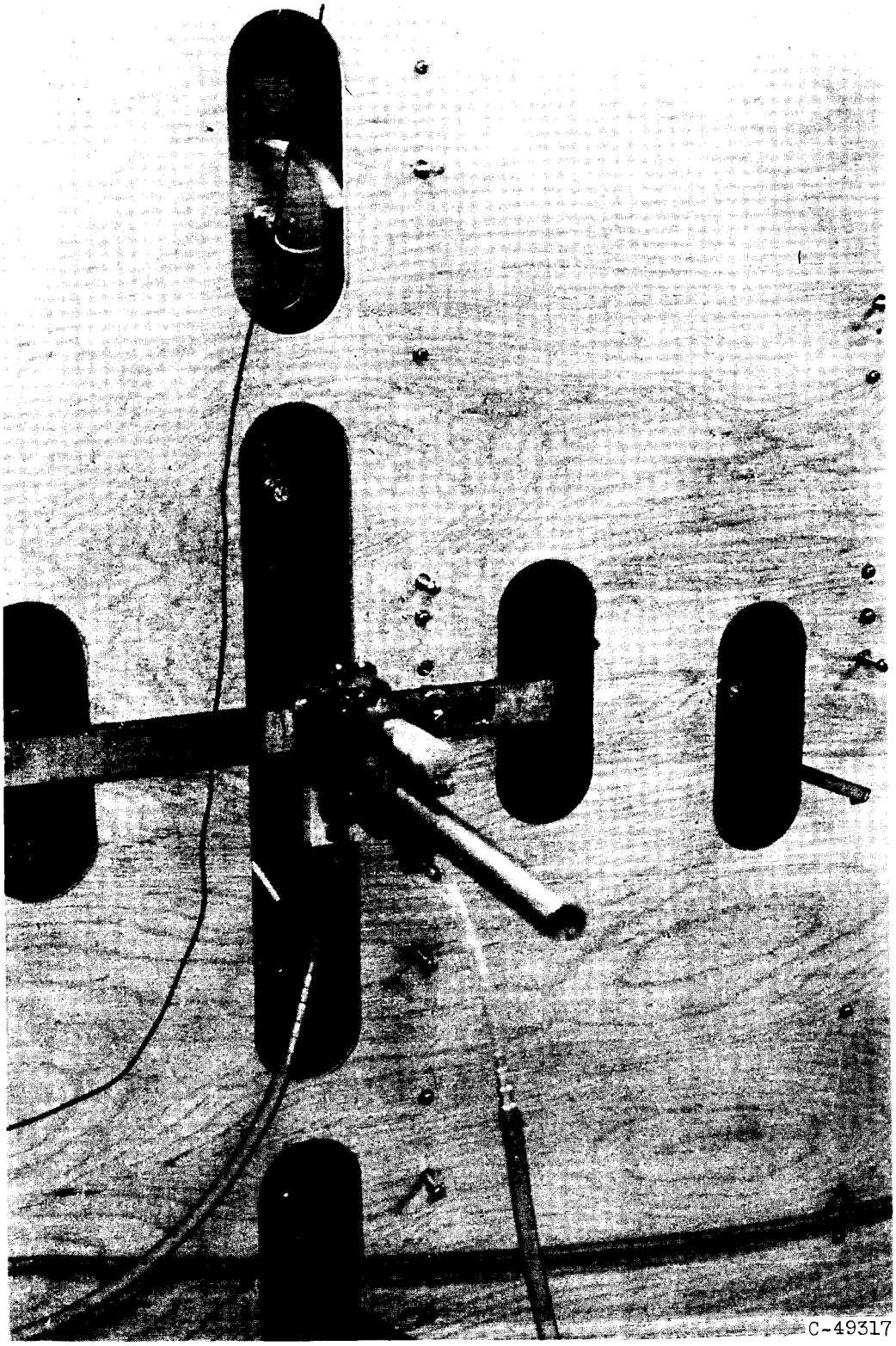

Figure 2. - Probe traversing mechanism mounted on tunnel wall.

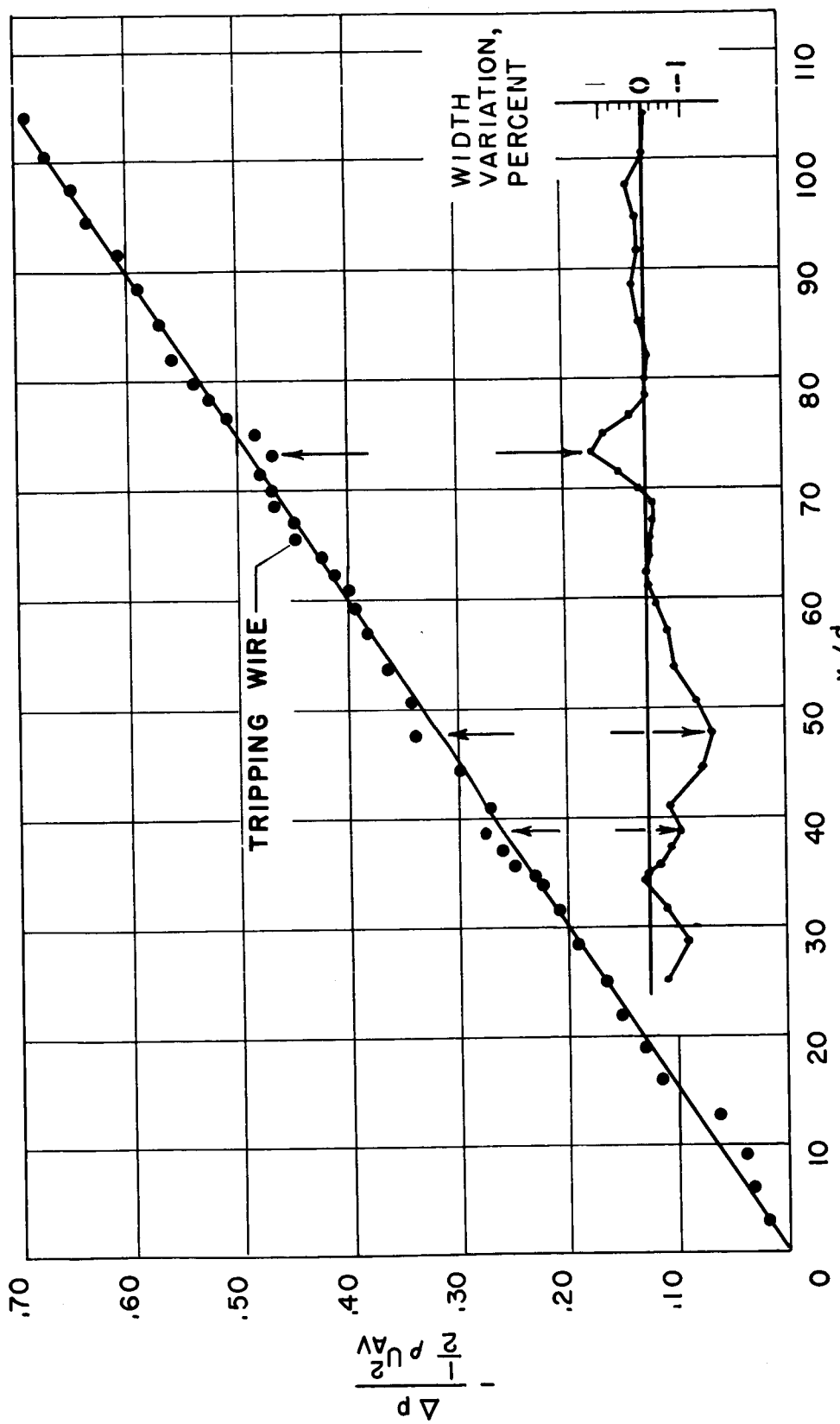

Figure 3. - Static-pressure drop along channel length. Average channel width, d_{av}, 3.856.

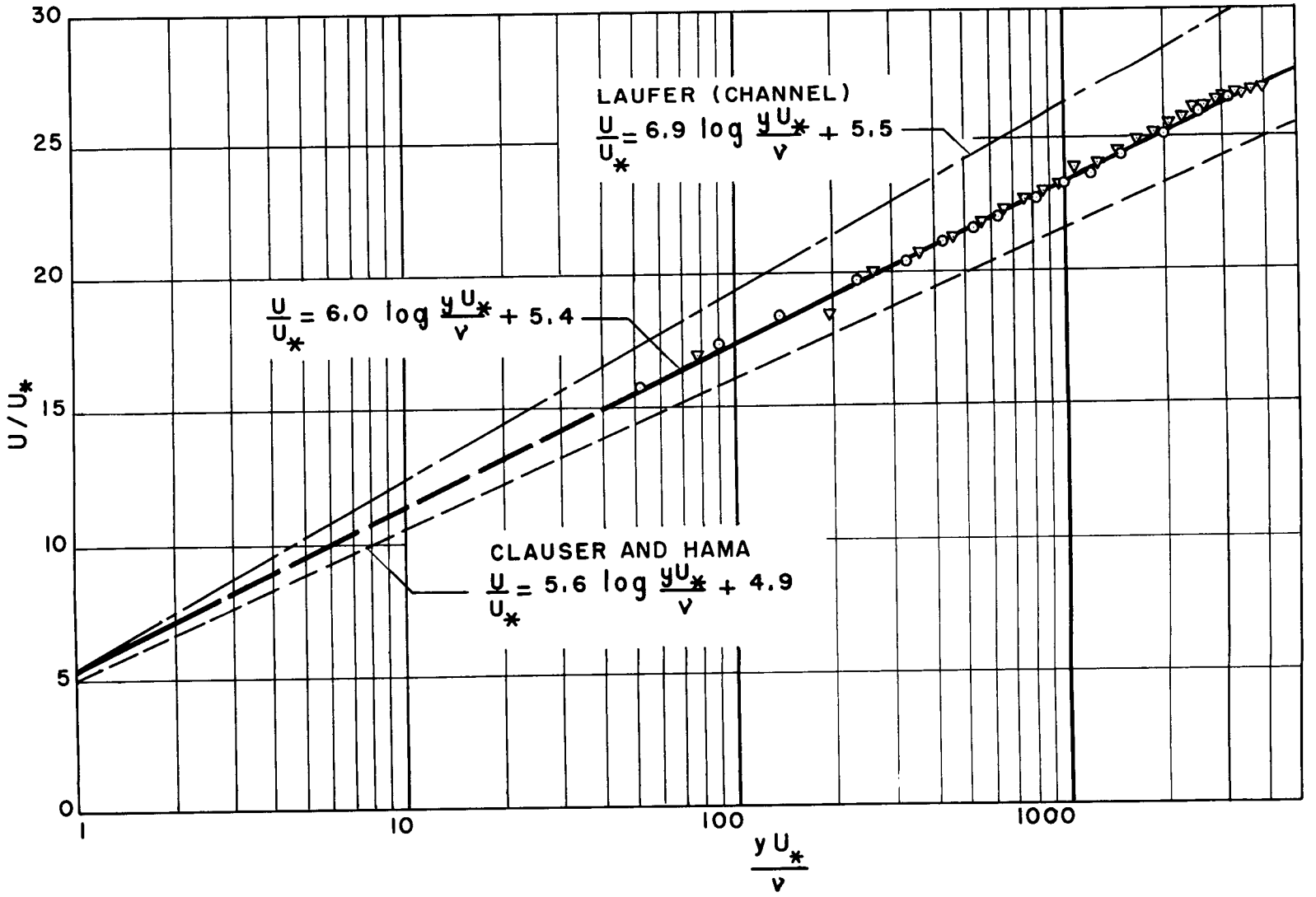

Figure 4. - Logarithmic representation of mean-velocity distribution.

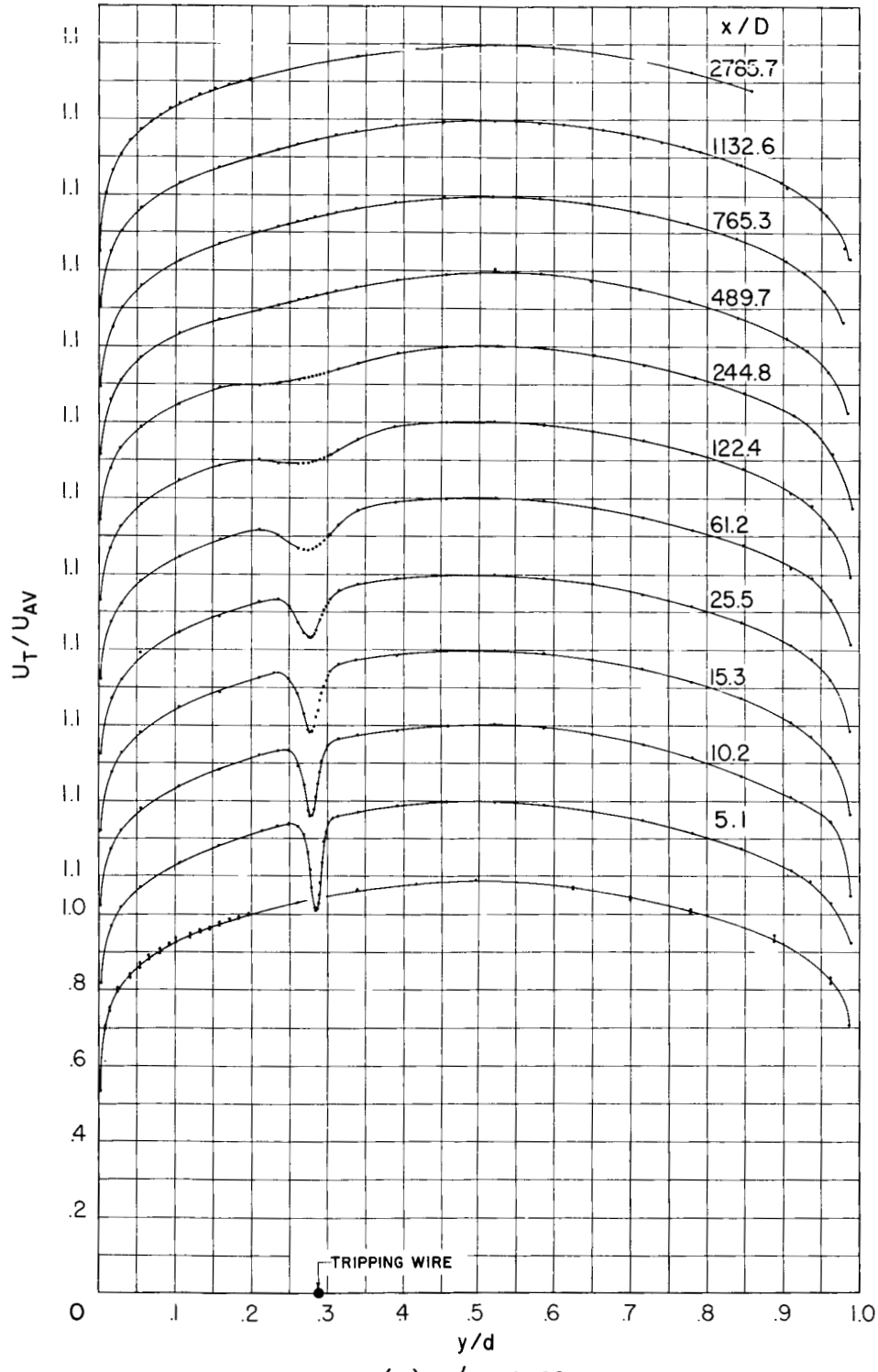

(a) η/d, 0.29.

Figure 5. - Dimensionless velocity distribution in wake. D/d, 0.0127.

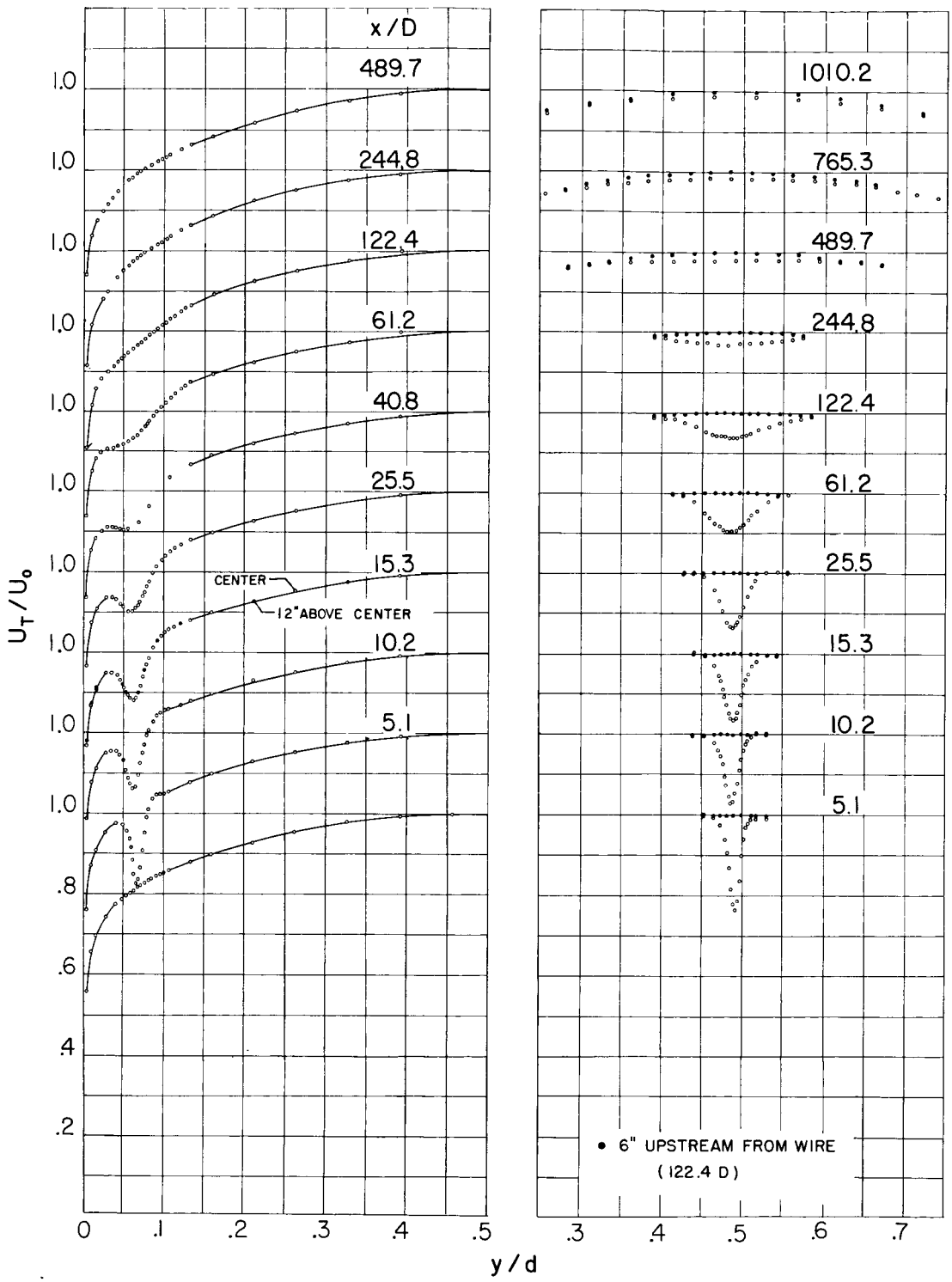

(b) η/d, 0.0715.

(c) η/d, 0.496.

Figure 5. - Concluded.

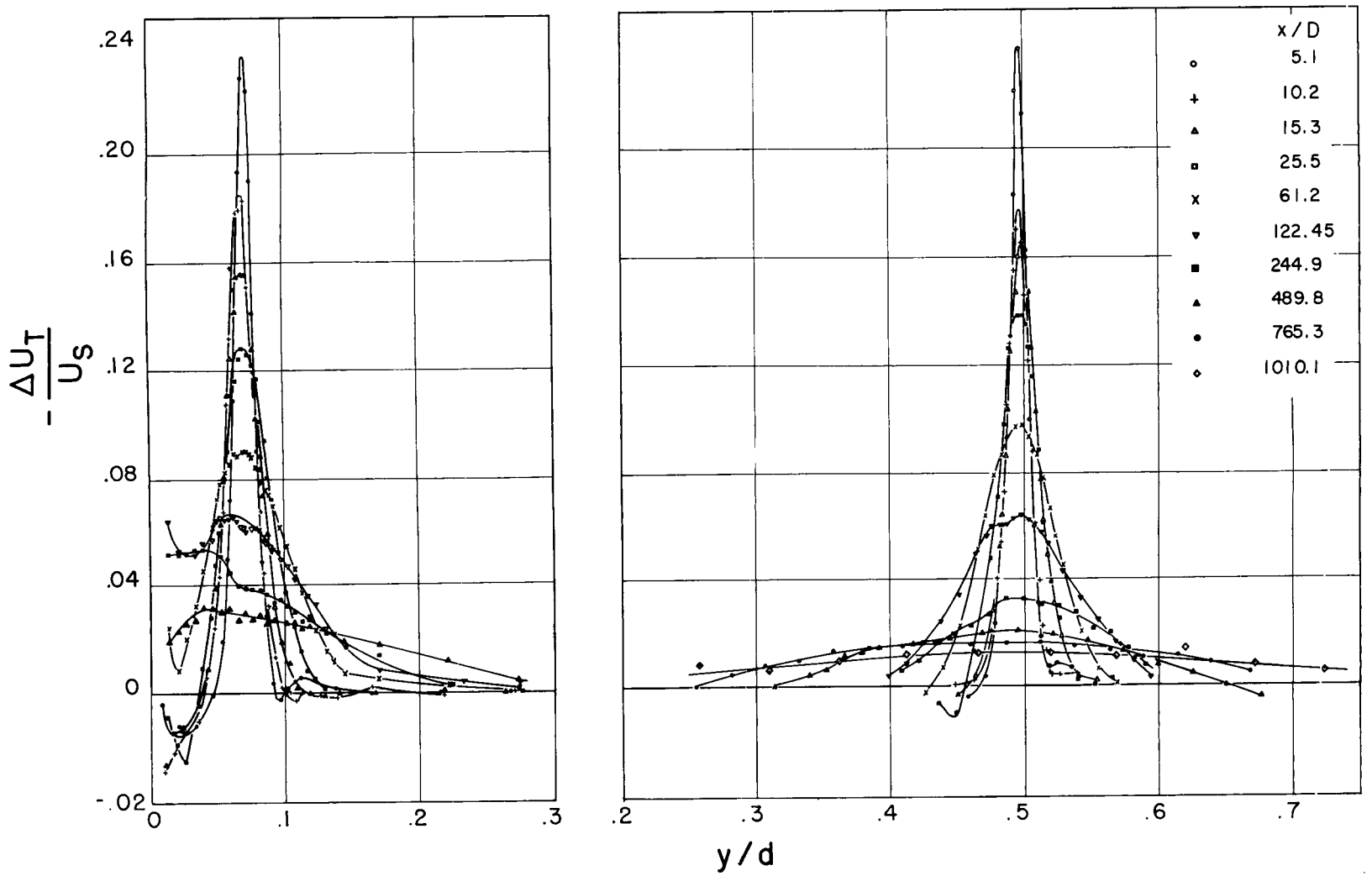

(a) η/d, 0.0715.

(b) η/d, 0.496.

Figure 6. - Percent mean-velocity deficiency in wake.

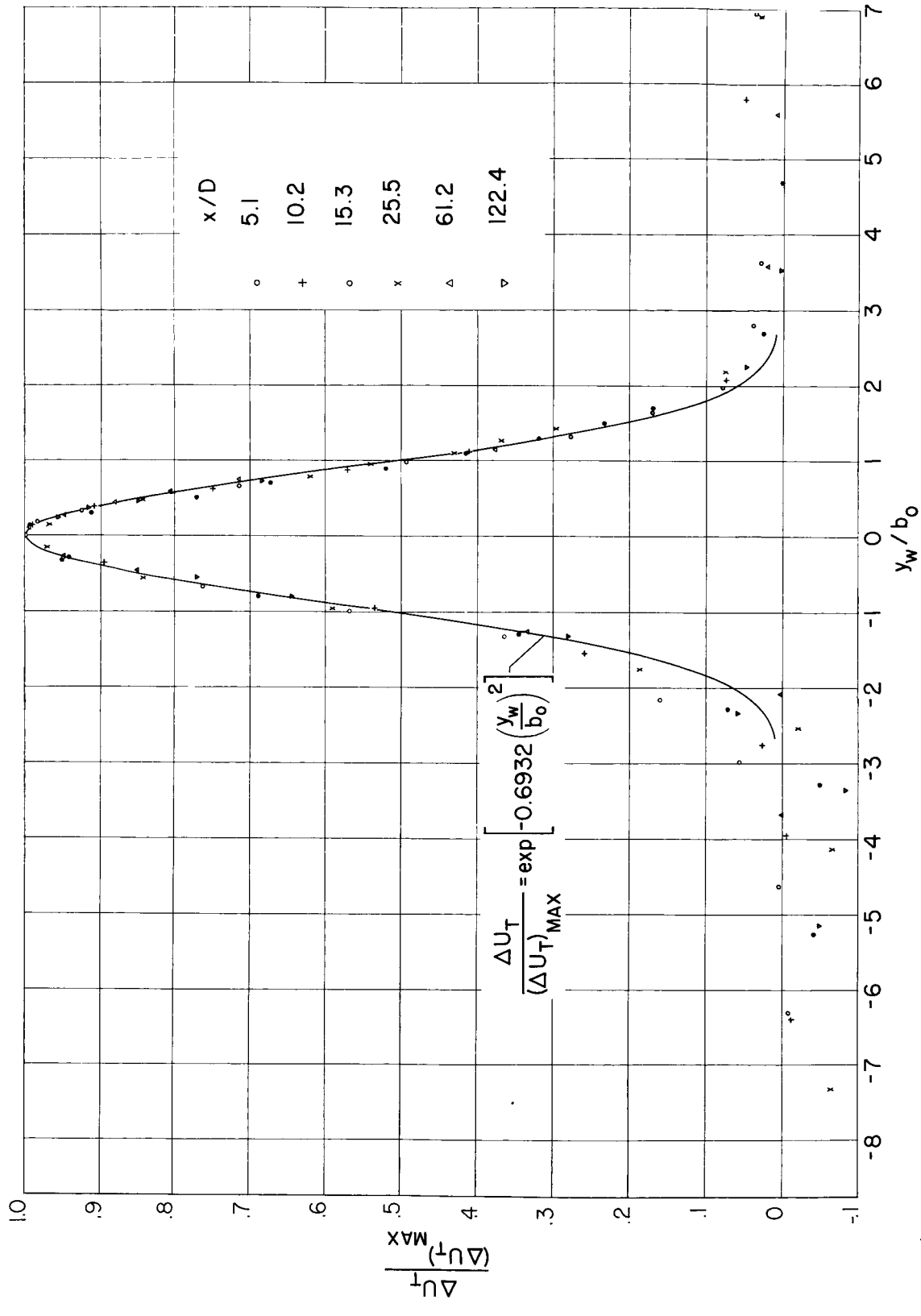

Figure 7. - Dimensionless form of velocity deficiency in wake. η/d, 0.29; D/d, 0.0127.

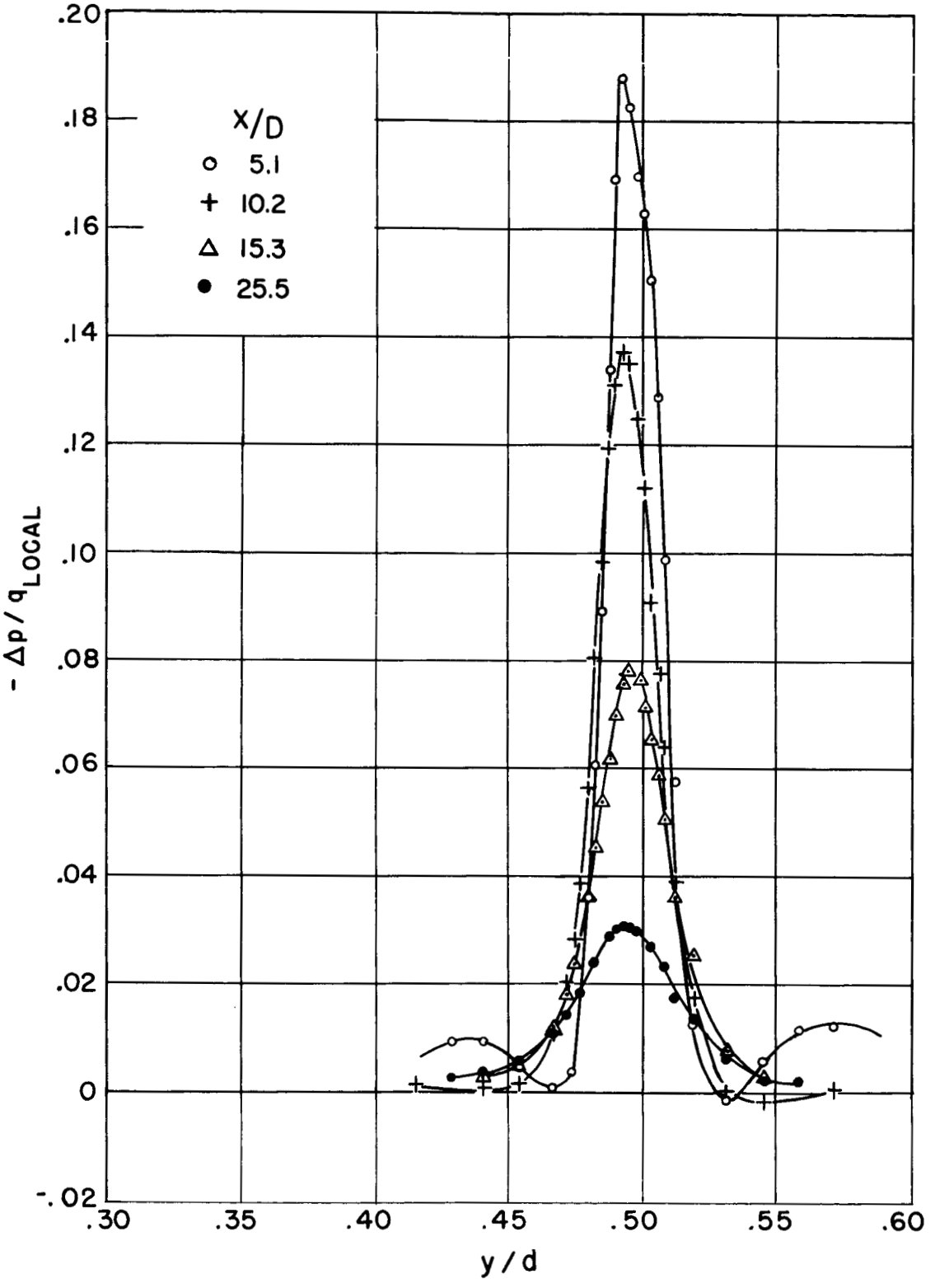

Figure 8. - Static-pressure drop in wake. η/d, 0.496.

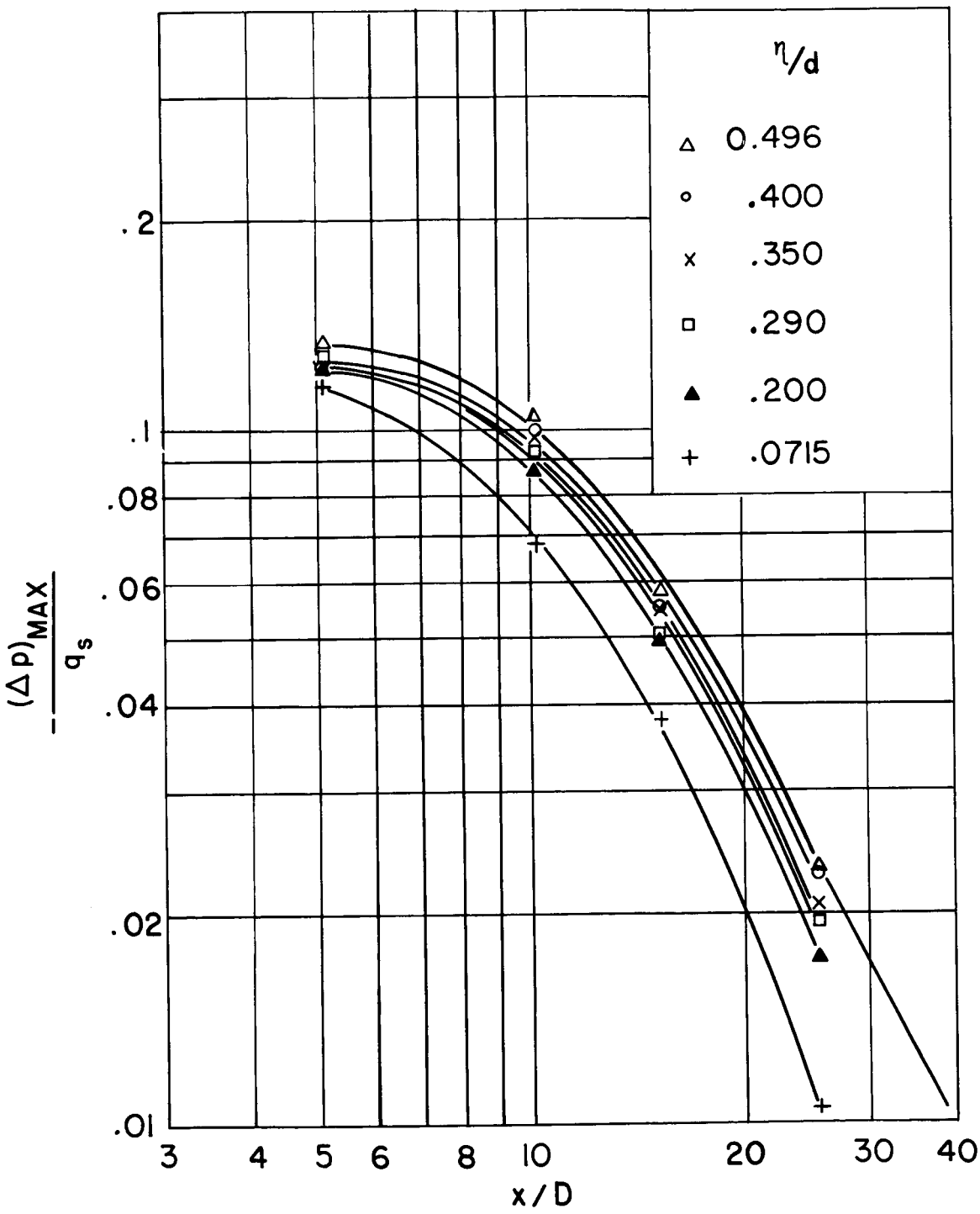

Figure 9. - Static-pressure recovery at center of wake.

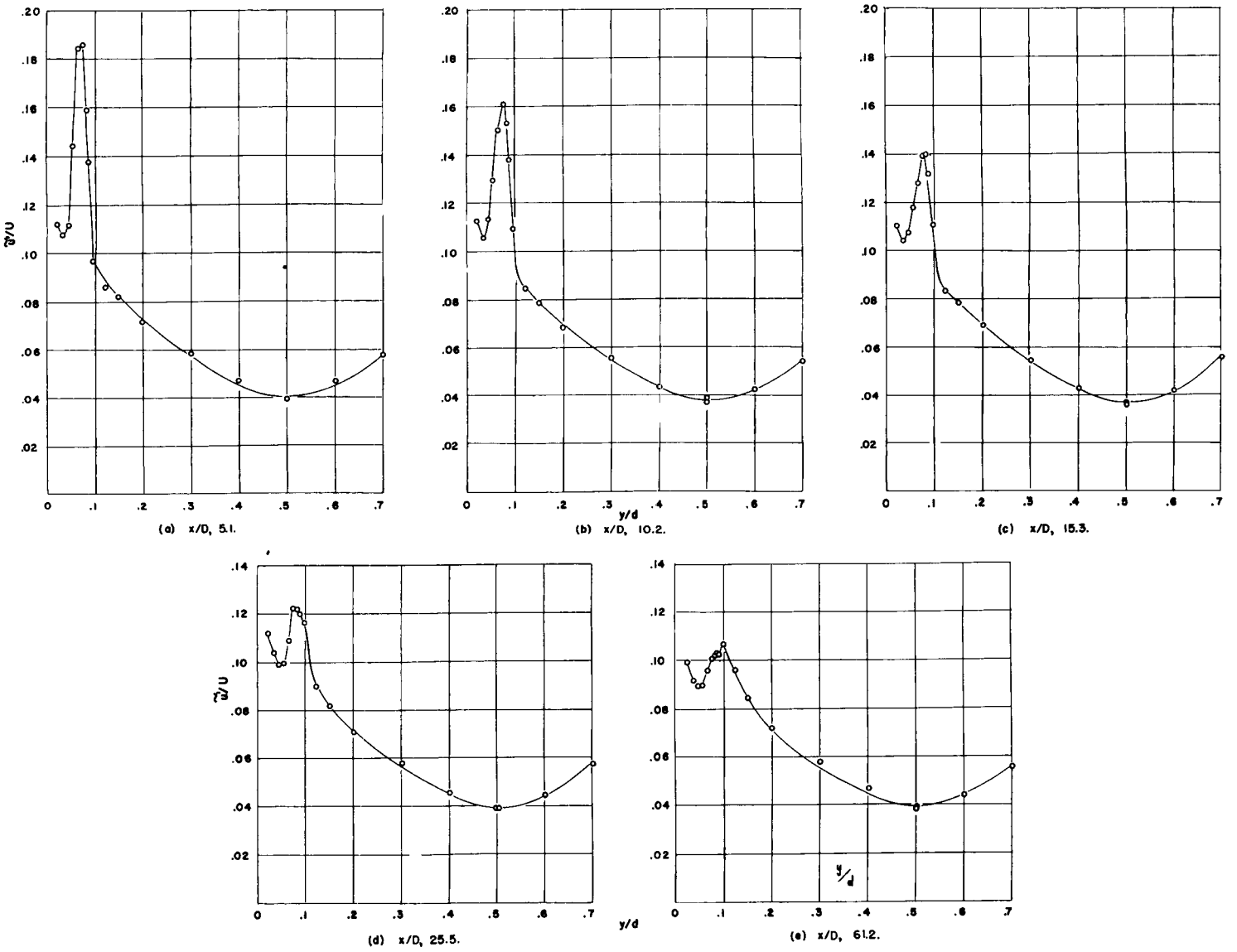

Figure 10. - Local turbulence intensity with tripping wire at $\eta/d = 0.072$.

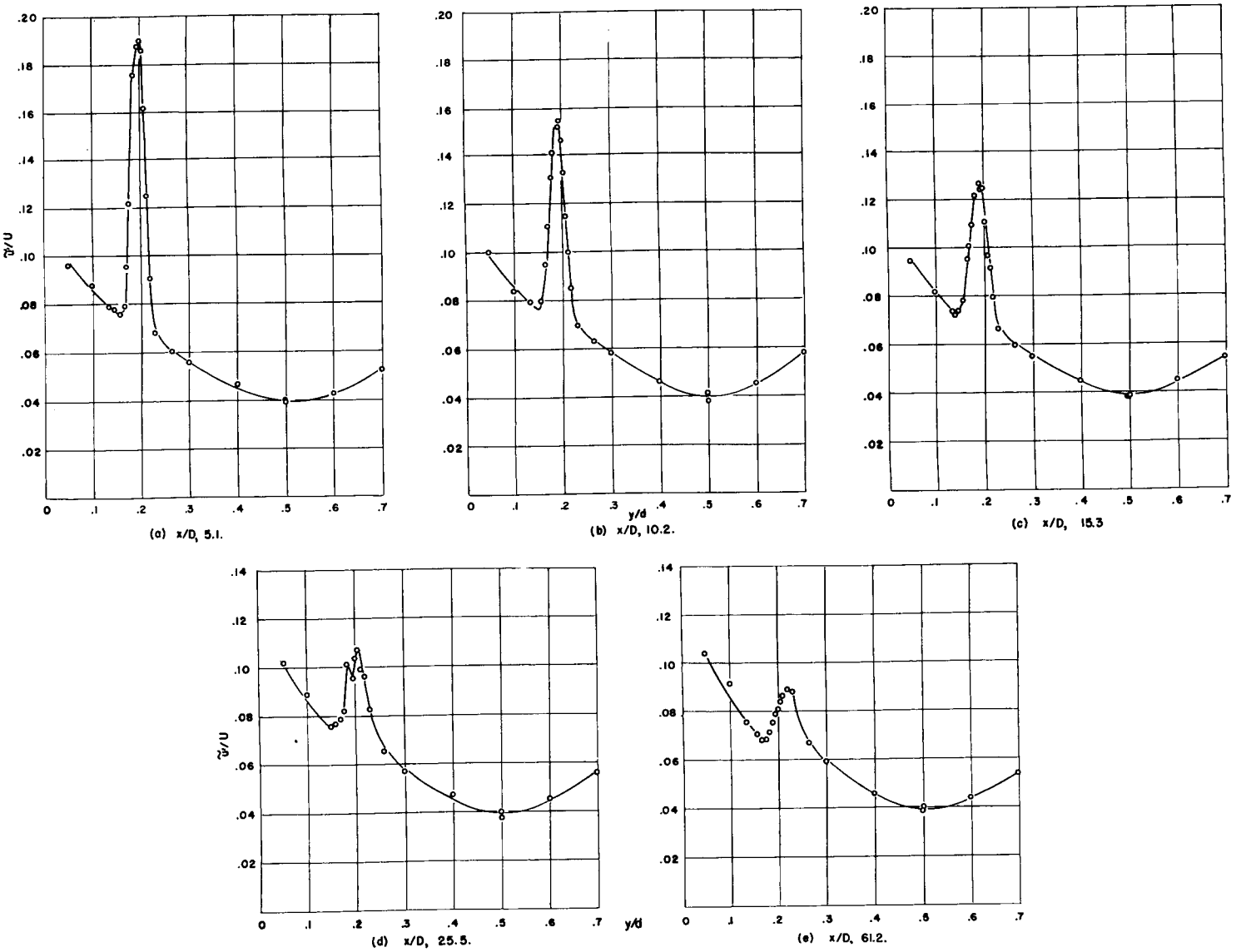

Figure 11. - Local turbulence intensity with tripping wire at $\eta/d = 0.20$.

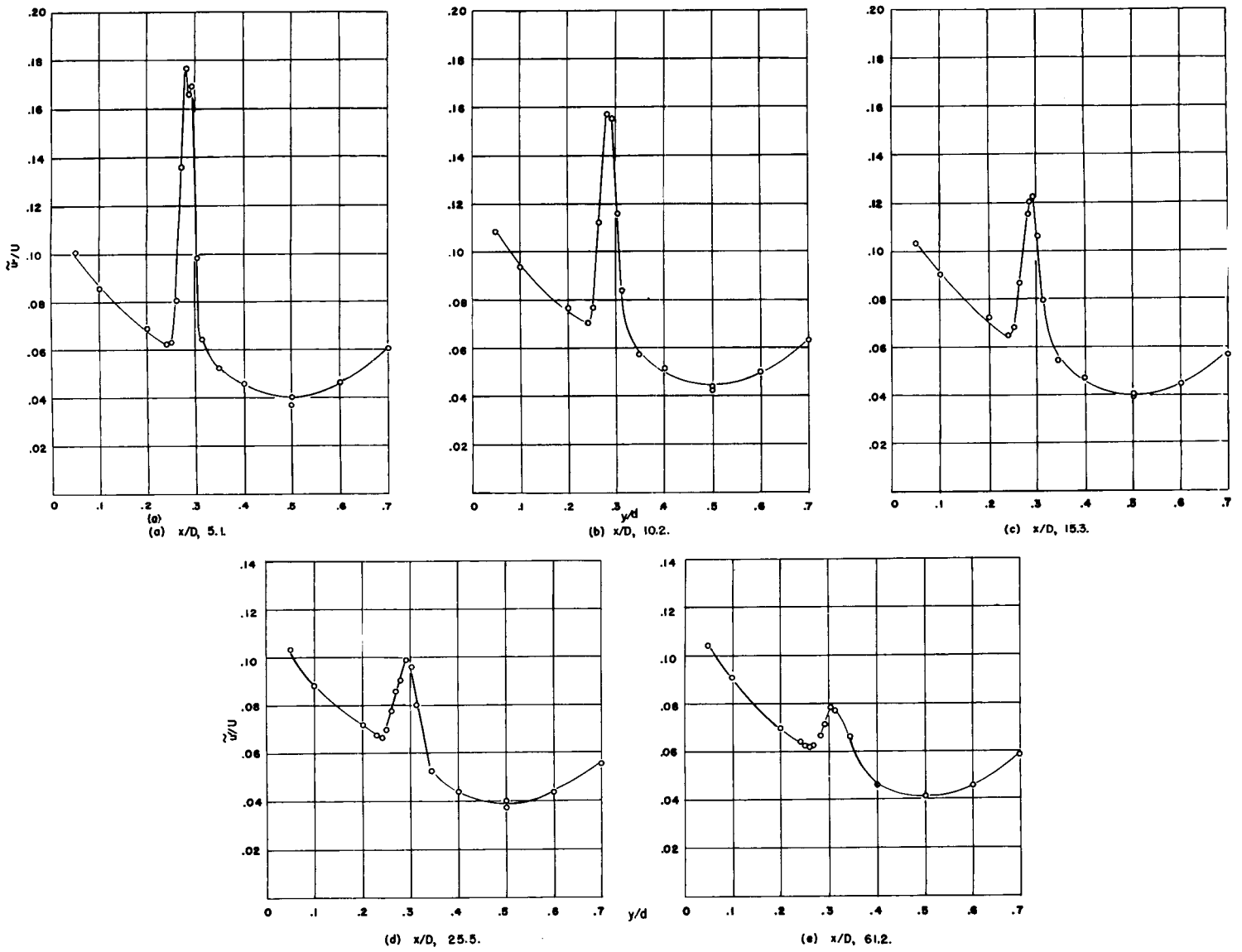

Figure 12. - Local turbulence intensity with tripping wire at $\eta/d = 0.292$.

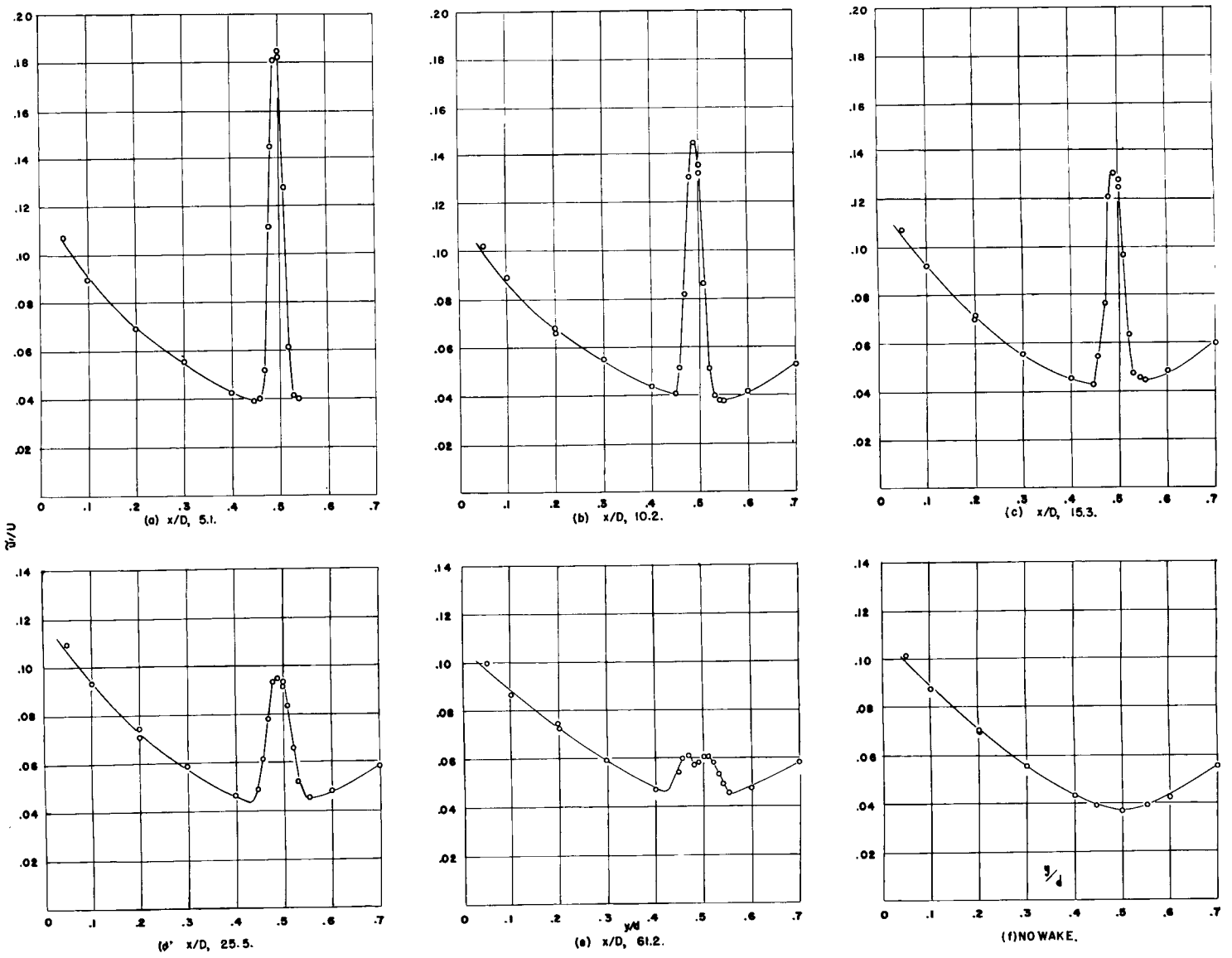

Figure 13. - Local turbulence intensity with tripping wire at $\eta/d = 0.50$.

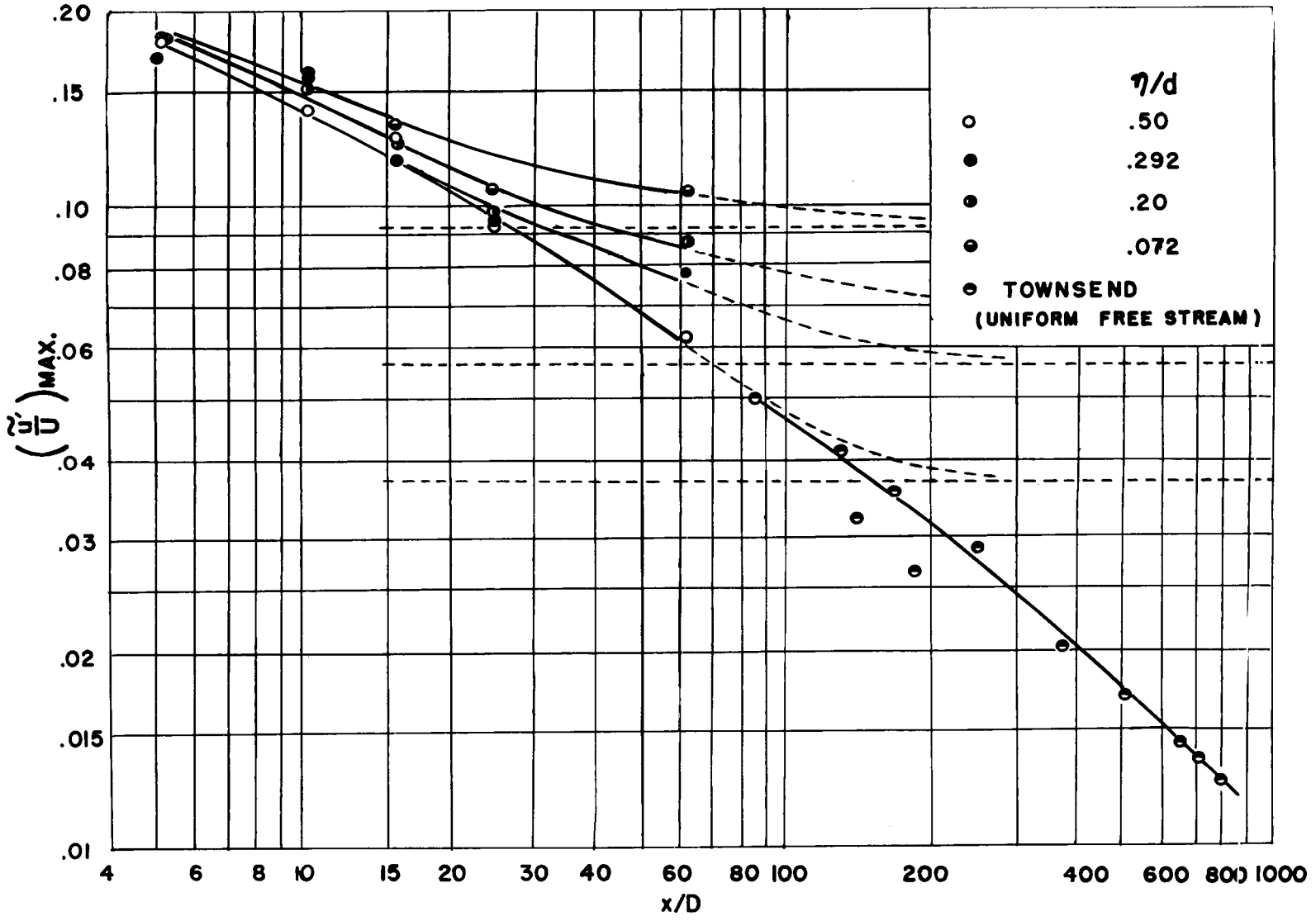

Figure 14. - Decay of turbulence in center of wake for various trip positions.

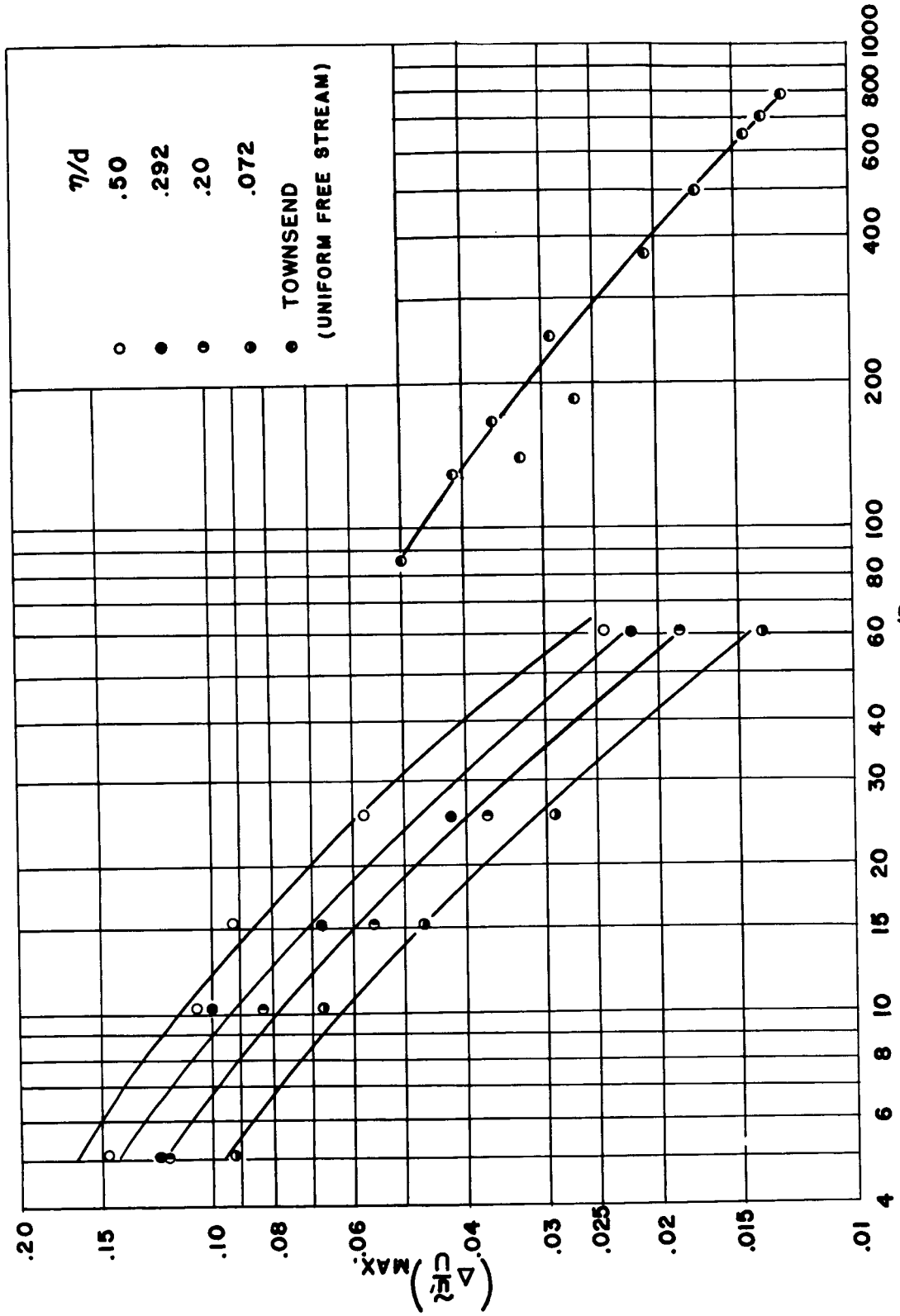

Figure 15. - Total decay of turbulence in center of wake.

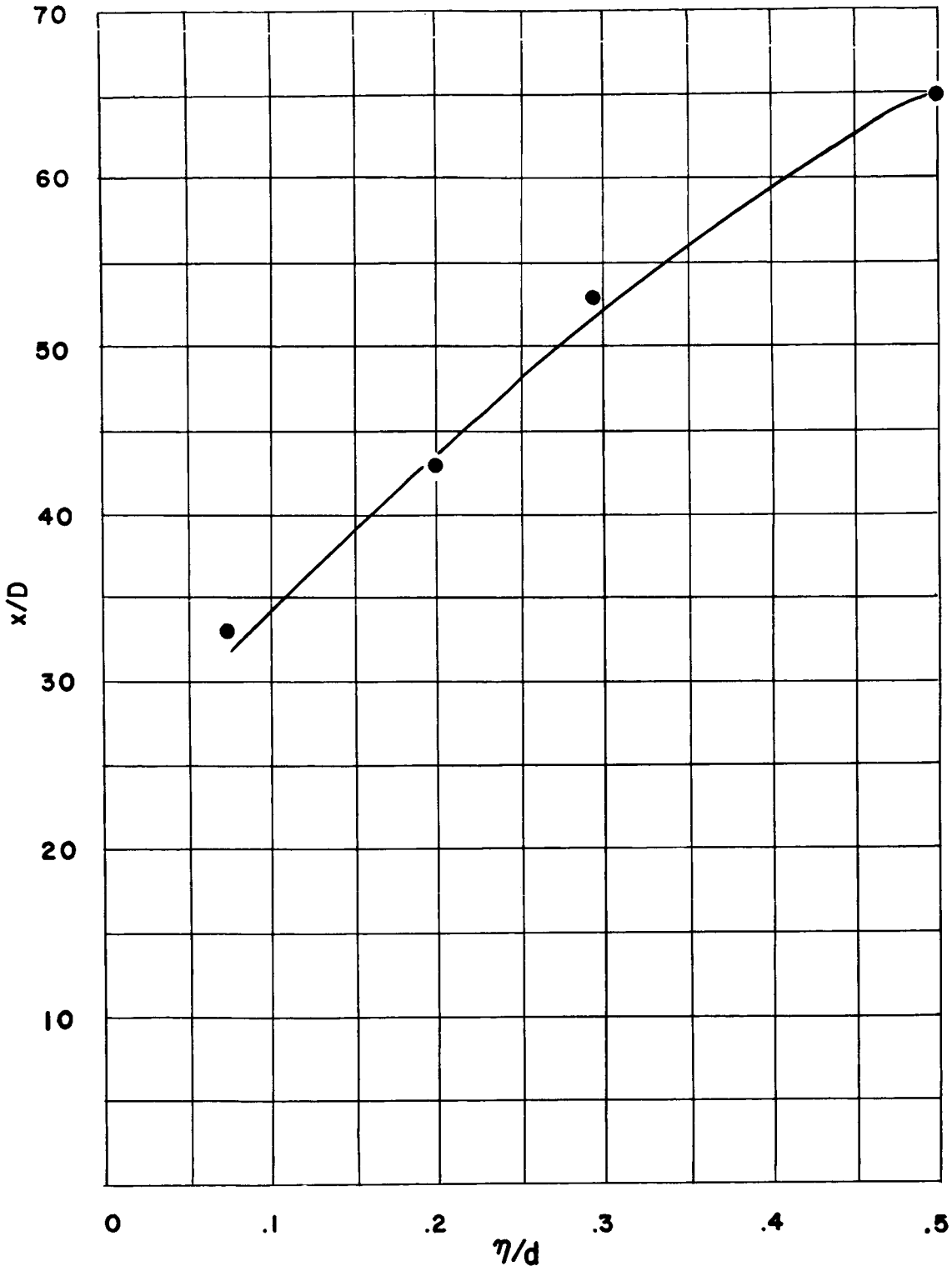

Figure 16. - Turbulence decay length to level $\Delta\left(\frac{\tilde{u}'}{U}\right) = 0.025$.

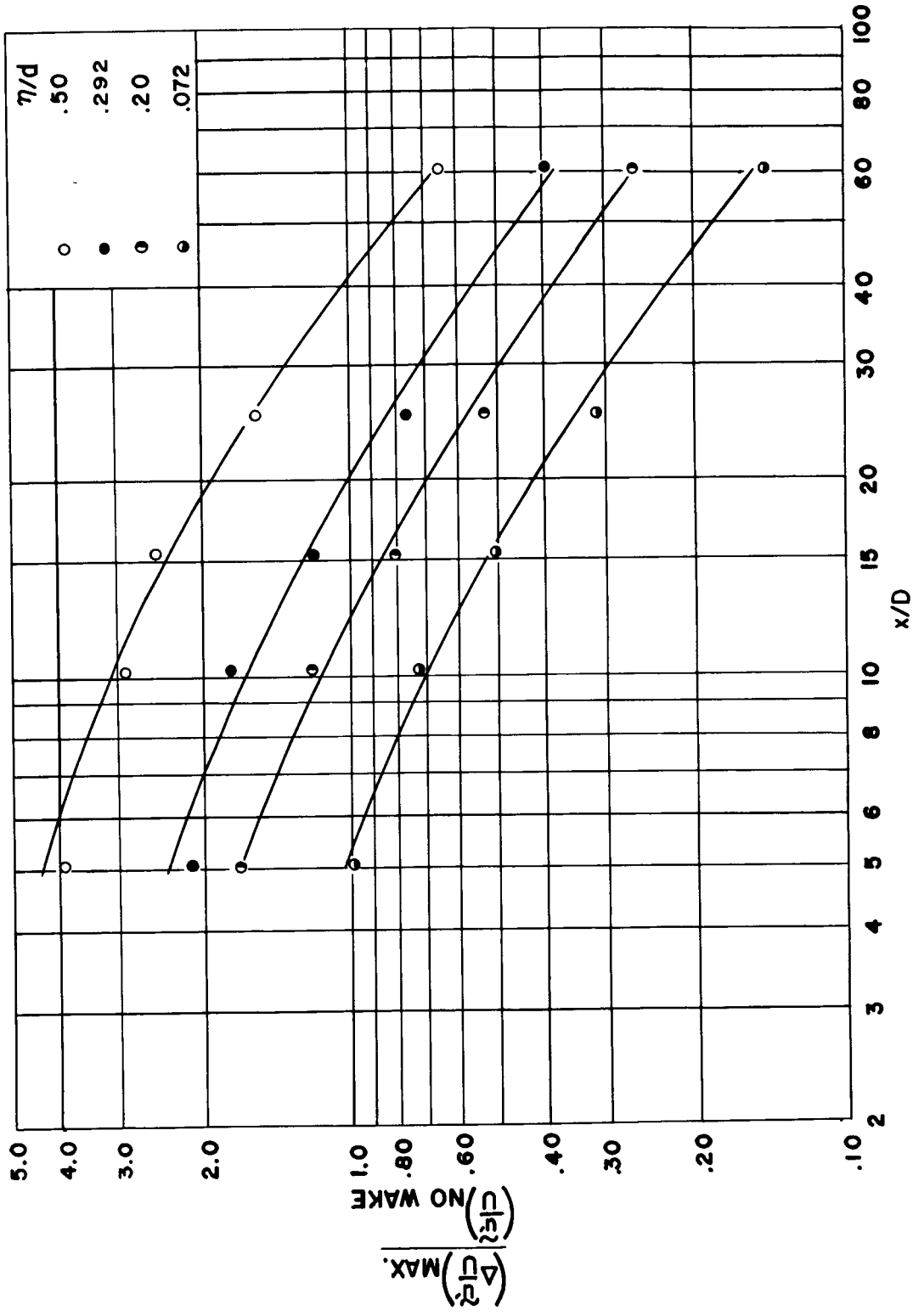

Figure 17. - Comparison of decay of turbulence in center of wake with final state.

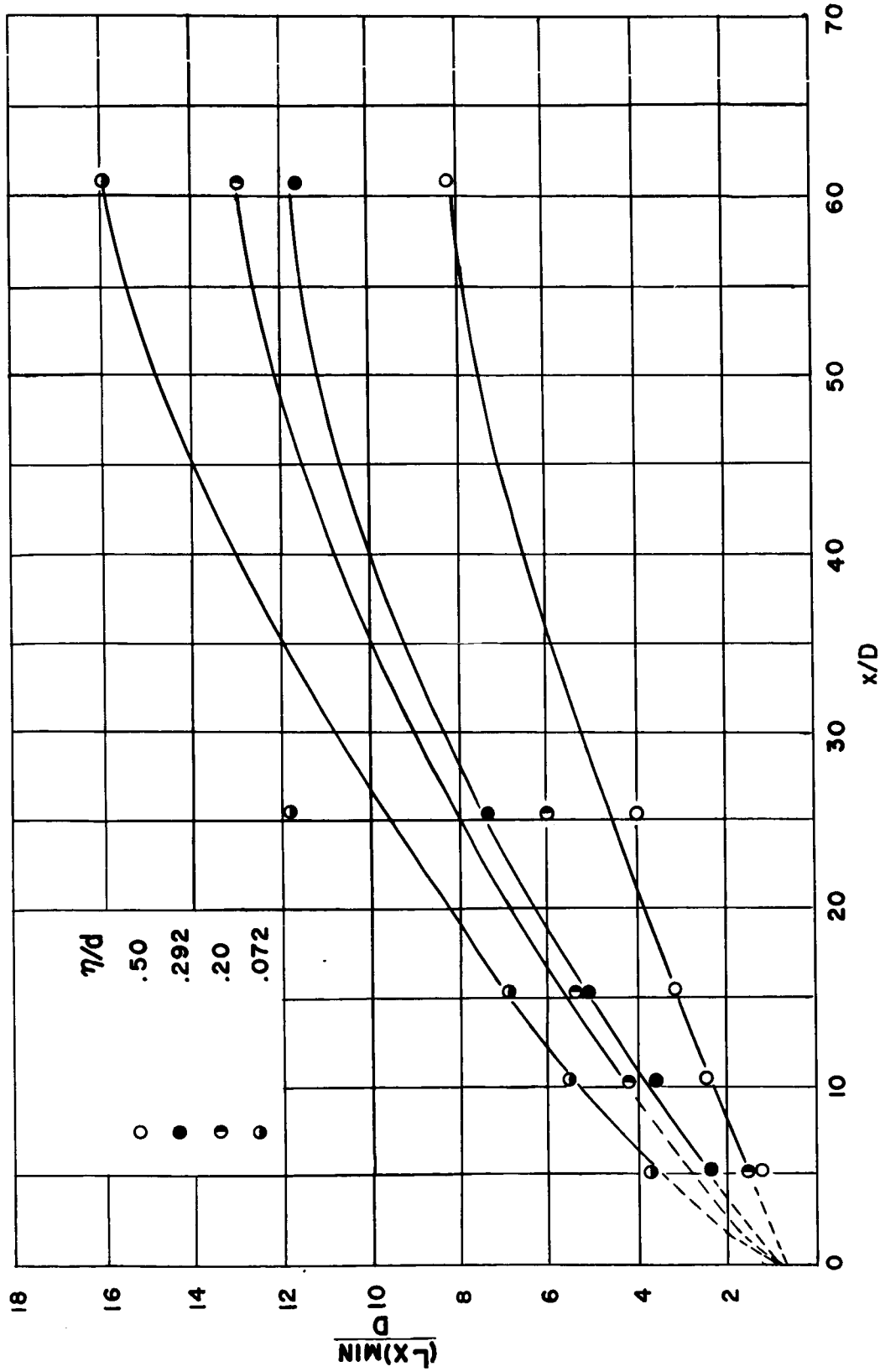

Figure 18. - Variation of $(L_x)_{min}$ in decay process.

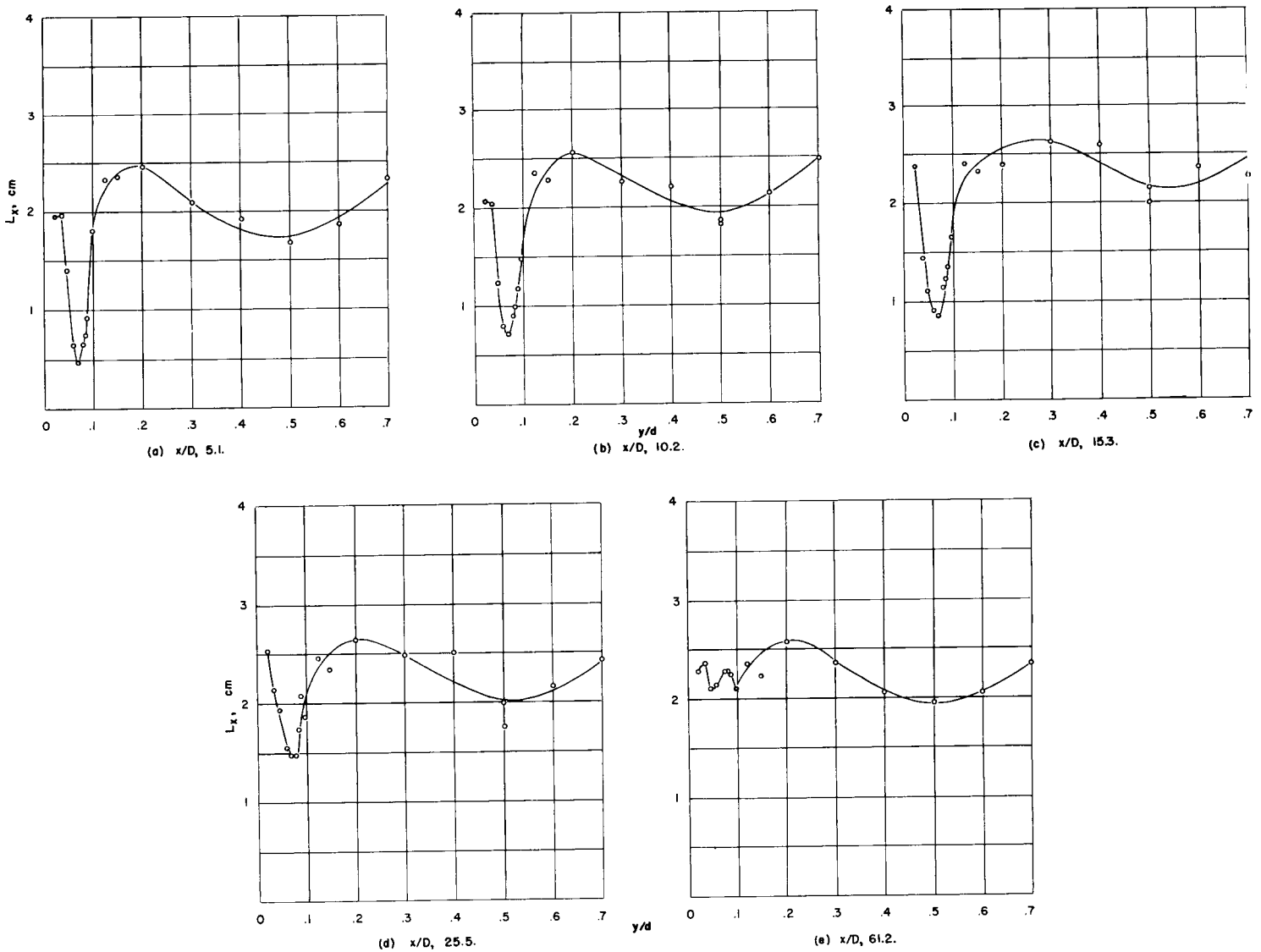

Figure 19. - Distributions of integral scale L_x with trippng wire at $\eta/d = 0.072$.

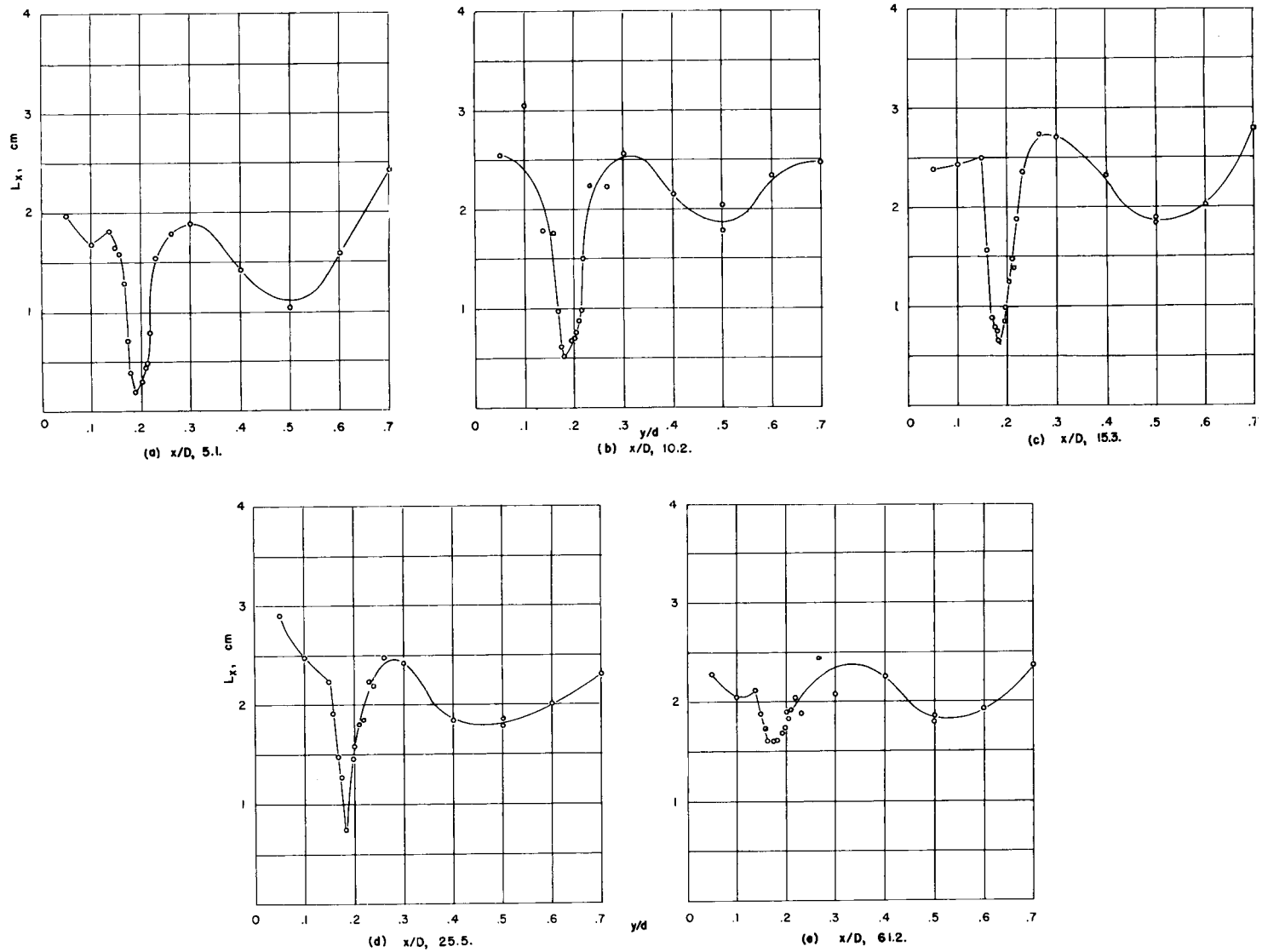

Figure 20. - Distributions of integral scale L_x with tripping wire at $\eta/d = 0.20$.

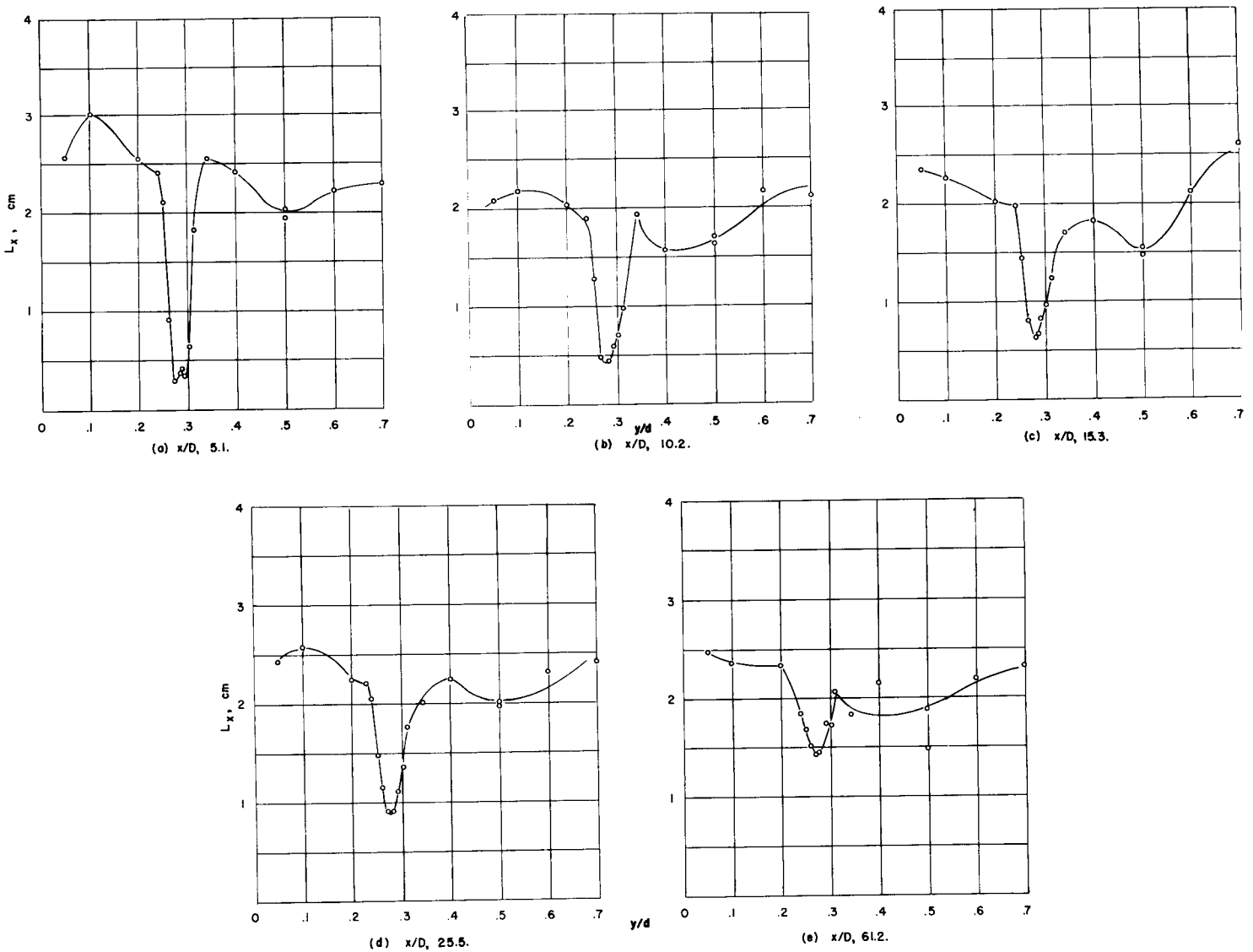

Figure 21. - Distributions of integral scale L_x with tripping wire at $\eta/d = 0.292$.

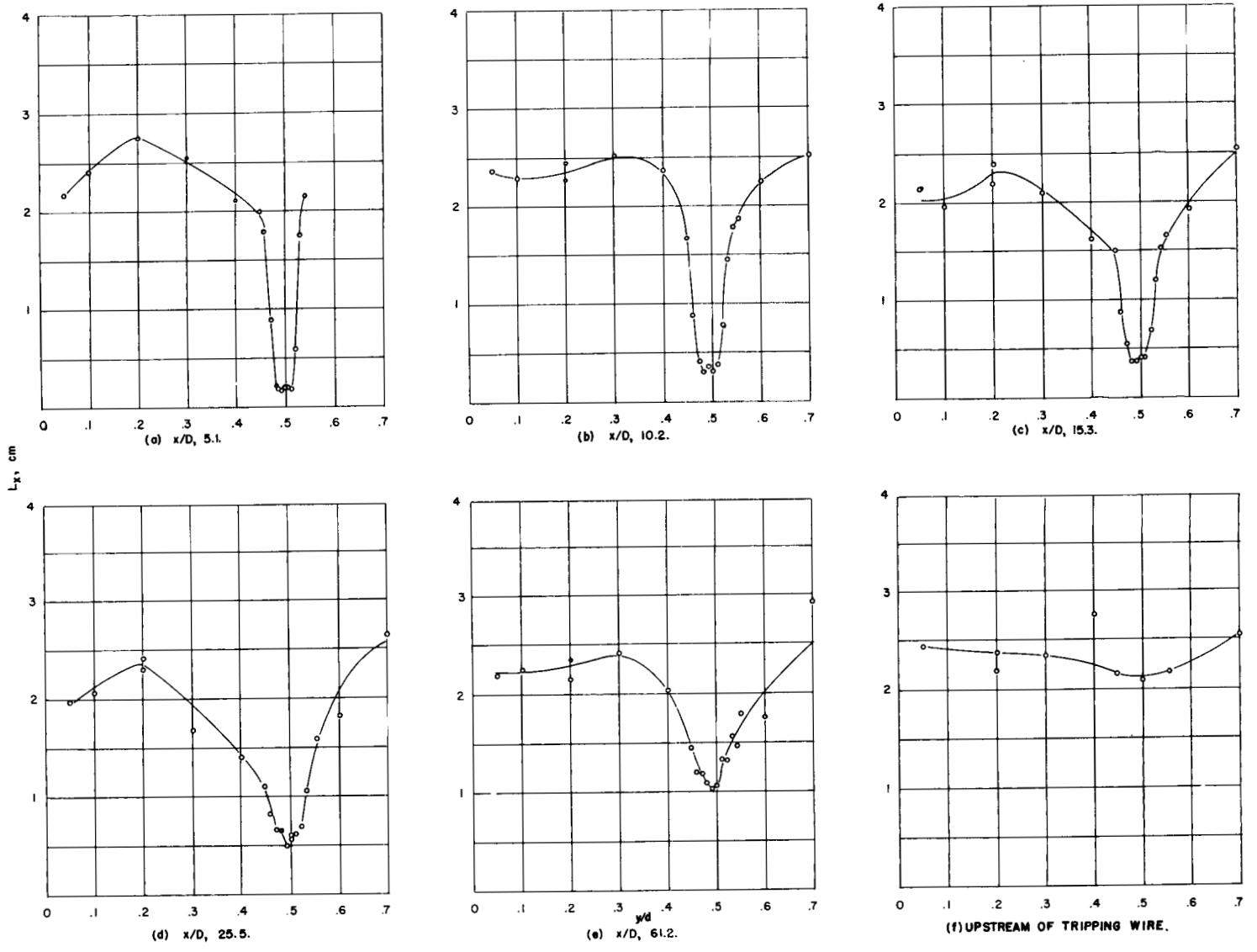

Figure 22. - Distributions of integral scale L_X with tripping wire at $\eta/d = 0.50$.

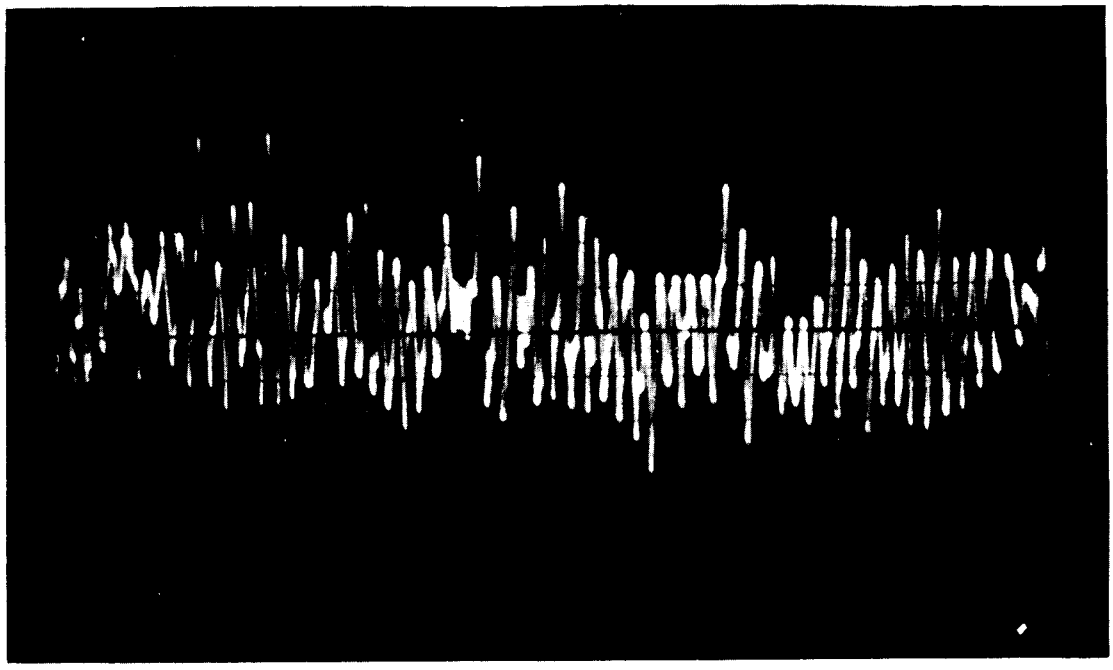

(a) In center of wake.

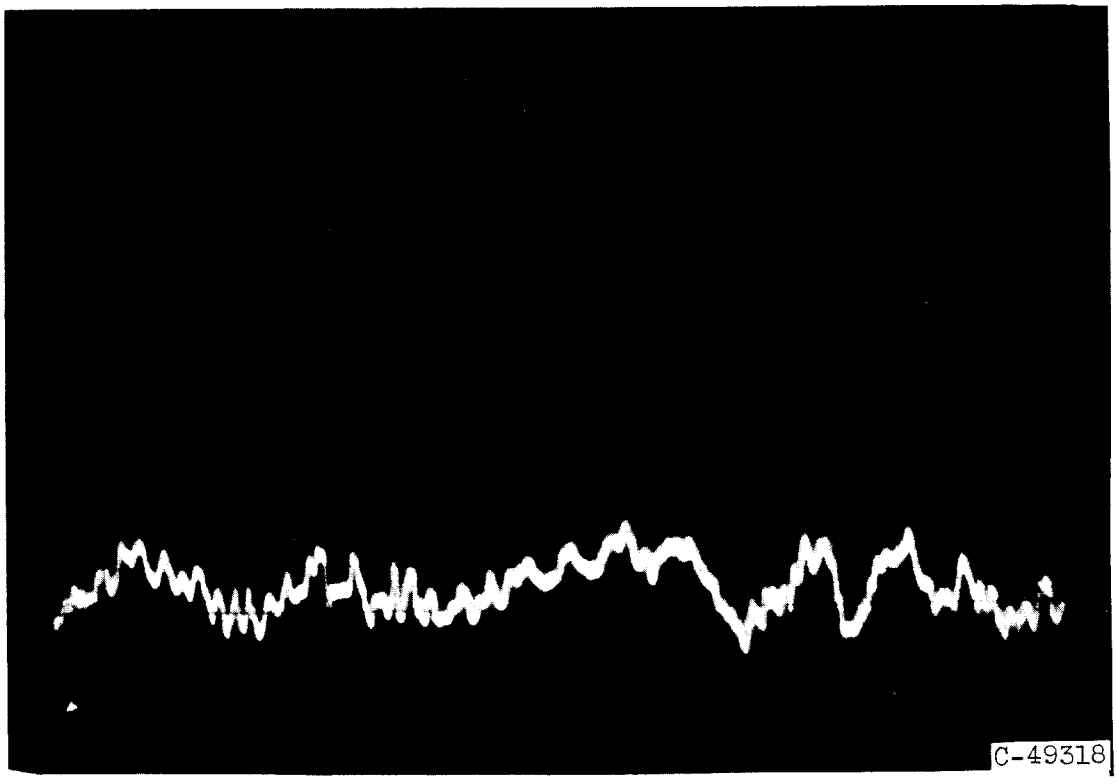

(b) Just outside wake; y/d, 0.026.

Figure 23. - Oscilloscope trace of u_1 (t) velocity fluctuation. η/d, 0.0715; x/D, 5.1

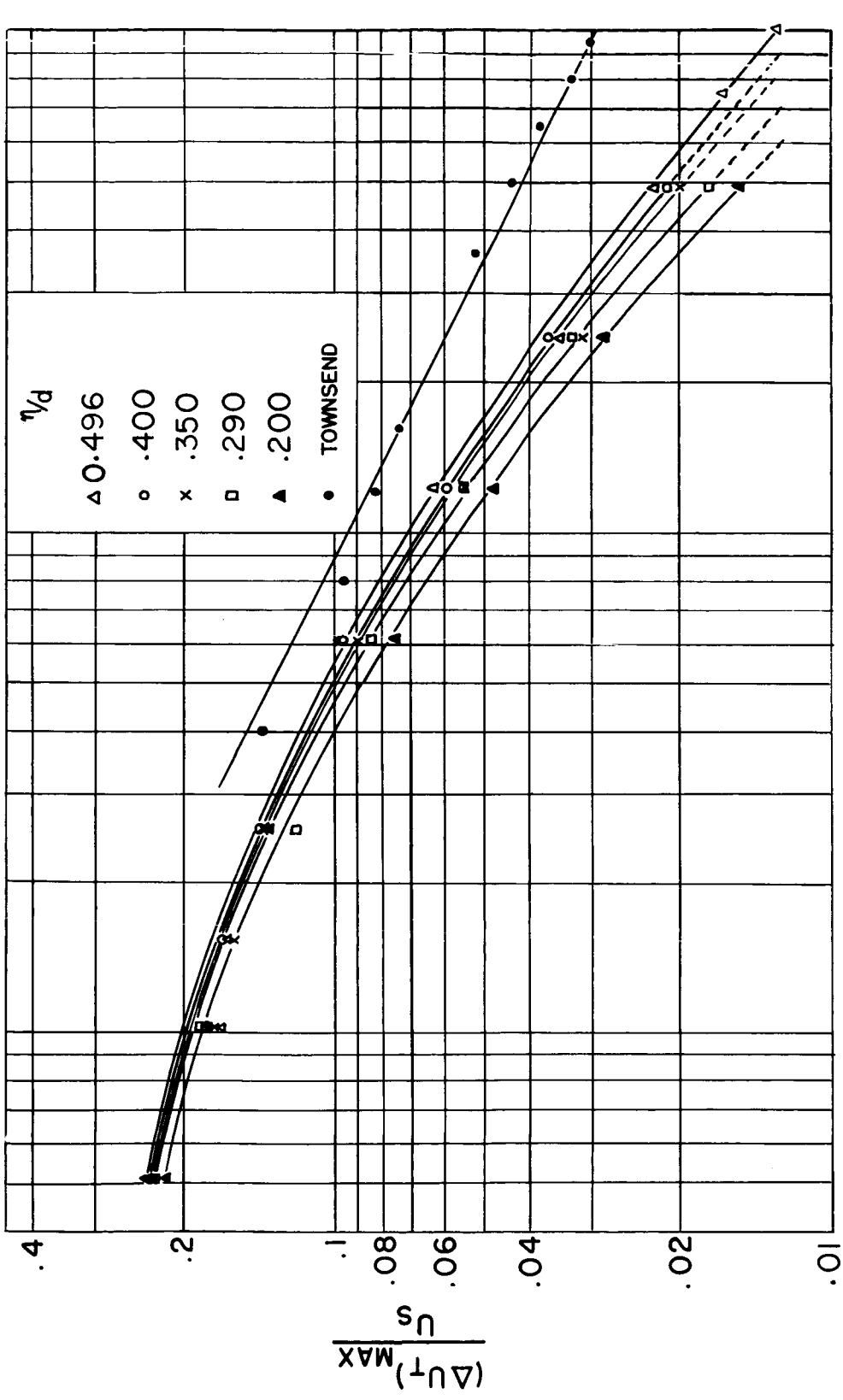

Figure 24. - Longitudinal decay of maximum velocity deficiency. Solid line through Townsend's points has slope of -1/2.

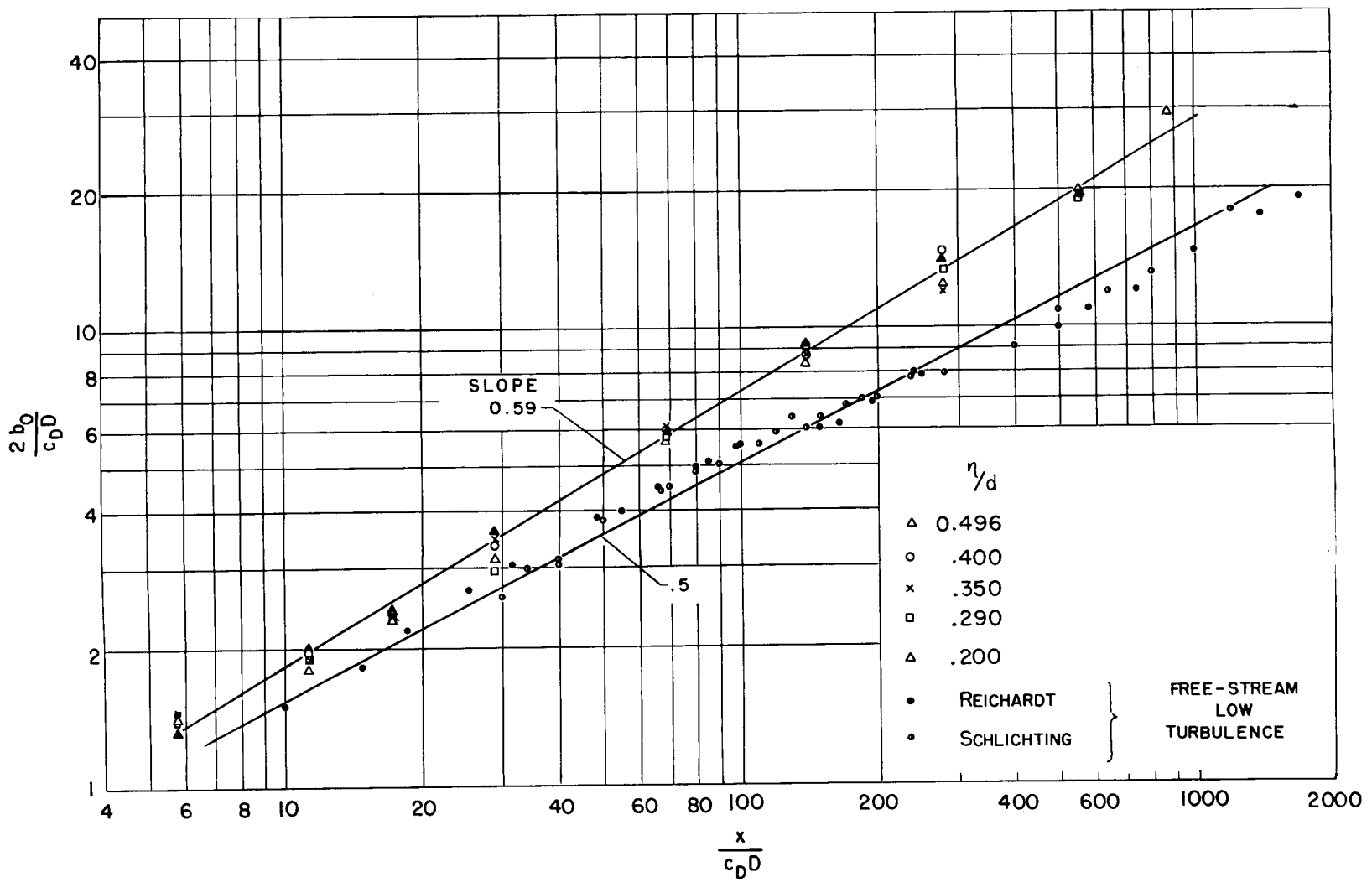

Figure 25. - Spread of wake in direction of flow.

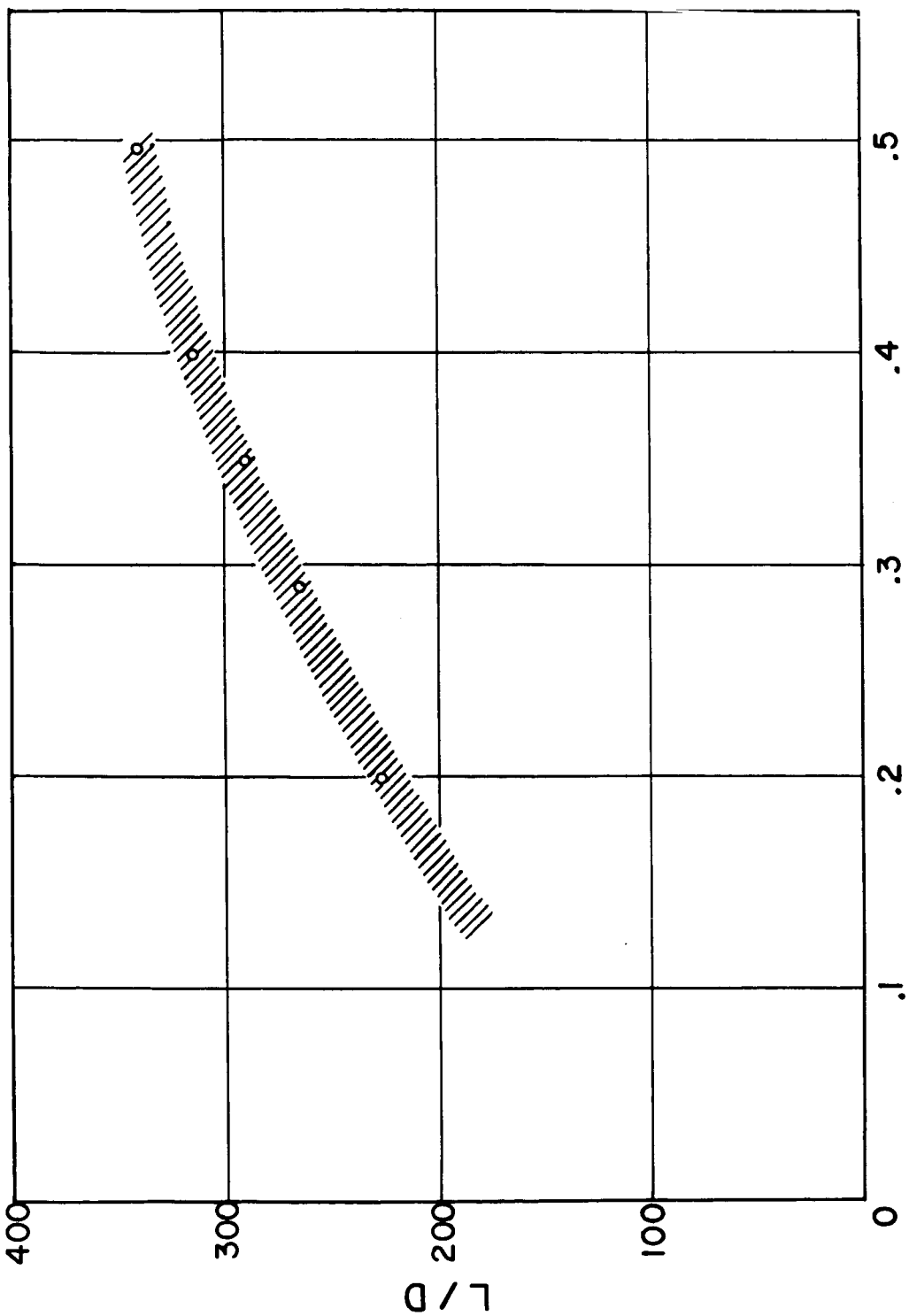

Figure 26. - Decay length across turbulent shear layer.

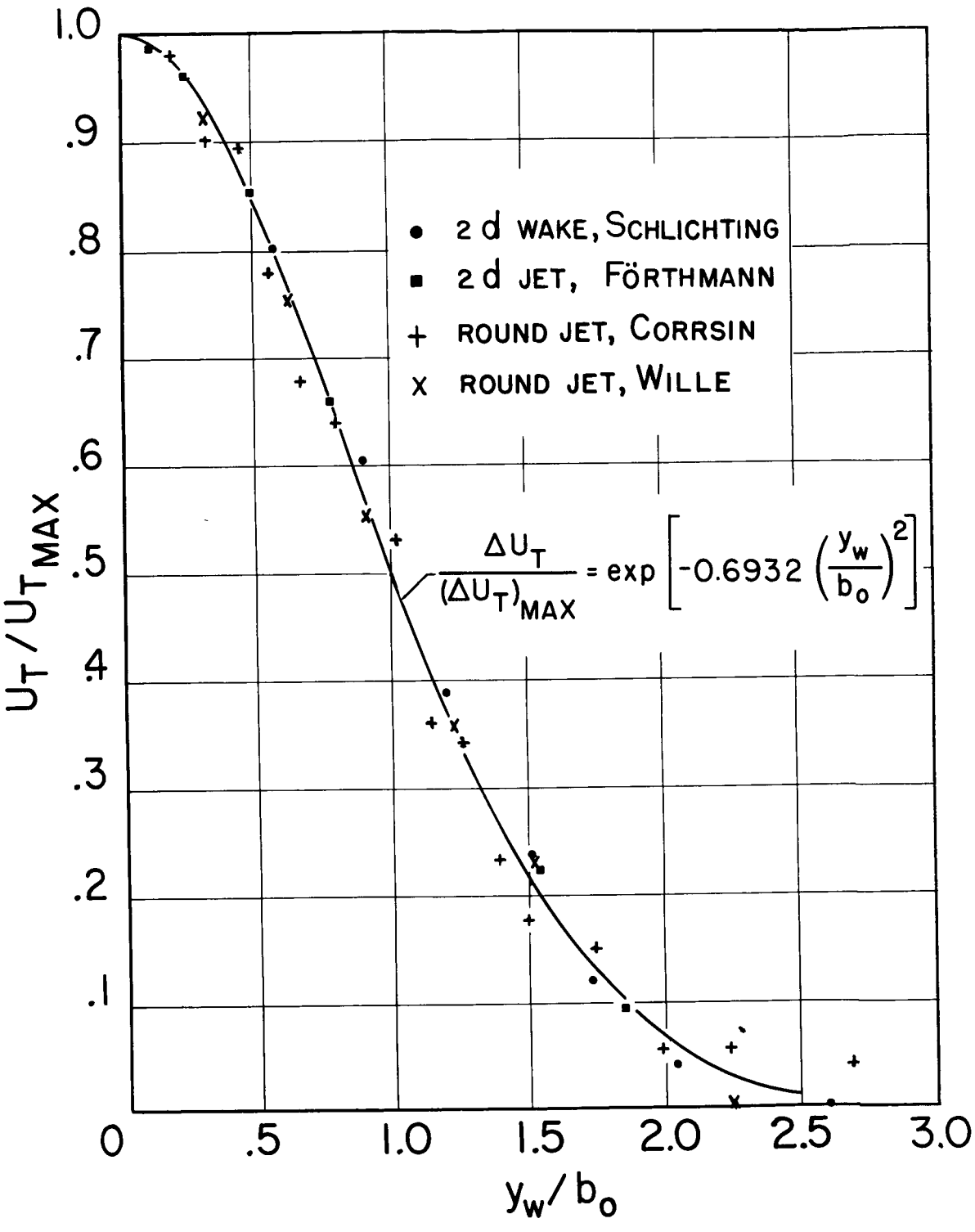

Figure 27. - Correlated experimental velocity distributions of fully developed wakes and jets.

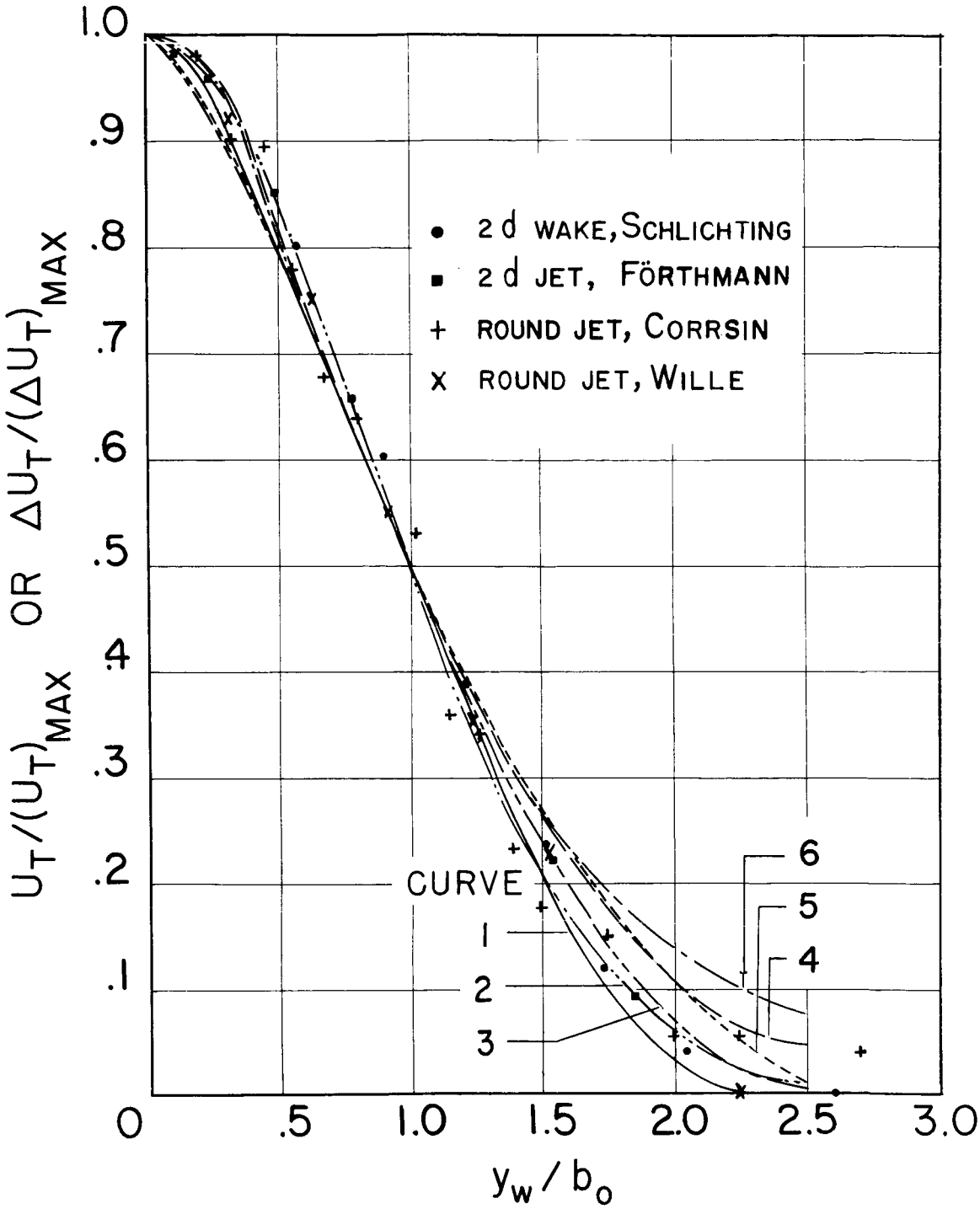

Figure 28. - Comparison of analytical solutions with experimental data for fully developed wakes and jets.